**Supplementary Information**

# Analysis of rare genetic variation underlying cardiometabolic diseases and traits among 200,000 individuals in the UK Biobank

Sean J. Jurgens[1,2,†], Seung Hoan Choi[1,†], Valerie N. Morrill[1,†], Mark Chaffin[1], James P. Pirruccello[1,3], Jennifer L. Halford[1], Lu-Chen Weng[1,3], Victor Nauffal[1,3], Carolina Roselli[1], Amelia W. Hall[1,3], Matthew T. Oetjens[4], Braxton Lagerman[5], David P. vanMaanen[5], Regeneron Genetics Center[6,*], Krishna G. Aragam[1,3], Kathryn L. Lunetta[7,8], Christopher M. Haggerty[5,9], Steven A. Lubitz[1,3,10,#] & Patrick T. Ellinor[1,3,10,#]

1. Cardiovascular Disease Initiative, The Broad Institute of MIT and Harvard, Cambridge, MA, USA
2. Department of Experimental Cardiology, Amsterdam UMC, University of Amsterdam, Amsterdam, NL
3. Cardiovascular Research Center, Massachusetts General Hospital, Boston, MA, USA
4. Autism & Developmental Medicine Institute, Geisinger, Danville, PA, USA
5. Department of Translational Data Science and Informatics, Geisinger, Danville, PA, USA
6. Regeneron Genetics Center, Tarrytown, NY, USA
7. NHLBI and Boston University's Framingham Heart Study, Framingham, MA, USA
8. Department of Biostatistics, Boston University School of Public Health, Boston, MA, USA
9. Heart Institute, Geisinger, Danville, PA, USA.
10. Demoulas Center for Cardiac Arrhythmias, Massachusetts General Hospital, Boston, MA, USA

† Contributed equally to this work.
* List of consortium authors and their affiliations appear at the end of the main manuscript document
# Jointly supervised this work.

37

## Supplementary Note

## 1. Consortium Author List and Contribution Statements

**Regeneron Genetics Center**

All authors/contributors are listed in alphabetical order.

RGC Management and Leadership Team

Goncalo Abecasis, Aris Baras, Michael Cantor, Giovanni Coppola, Andrew Deubler, Aris Economides, Luca A. Lotta, John D. Overton, Jeffrey G. Reid, Alan Shuldiner, Katia Karalis and Katherine Siminovitch

Contribution: All authors contributed to securing funding, study design and oversight. All authors reviewed the final version of the manuscript.

Sequencing and Lab Operations

Christina Beechert, Caitlin Forsythe, Erin D. Fuller, Zhenhua Gu, Michael Lattari, Alexander Lopez, John D. Overton, Thomas D. Schleicher, Maria Sotiropoulos Padilla, Louis Widom, Sarah E. Wolf, Manasi Pradhan, Kia Manoochehri, Ricardo H. Ulloa.

Contribution: C.B., C.F., A.L., and J.D.O. performed and are responsible for sample genotyping. C.B, C.F., E.D.F., M.L., M.S.P., L.W., S.E.W., A.L., and J.D.O. performed and are responsible for exome sequencing. T.D.S., Z.G., A.L., and J.D.O. conceived and are responsible for laboratory automation. M.S.P., K.M., R.U., and J.D.O are responsible for sample tracking and the library information management system.

Genome Informatics

Xiaodong Bai, Suganthi Balasubramanian, Boris Boutkov, Gisu Eom, Lukas Habegger, Alicia Hawes, Shareef Khalid, Olga Krasheninina, Rouel Lanche, Adam J. Mansfield, Evan K. Maxwell, Mona Nafde, Sean O'Keeffe, Max Orelus, Razvan Panea, Tommy Polanco, Ayesha Rasool, Jeffrey G. Reid, William Salerno, Jeffrey C. Staples,

Contribution: X.B., A.H., O.K., A.M., S.O., R.P., T.P., A.R., W.S. and J.G.R. performed and are responsible for the compute logistics, analysis and infrastructure needed to produce exome and genotype data. G.E., M.O., M.N. and J.G.R. provided compute infrastructure development and operational support. S.B., S.K., and J.G.R. provide variant and gene annotations and their functional interpretation of variants. E.M., J.S., R.L., B.B., A.B., L.H., J.G.R. conceived and are responsible for creating, developing, and deploying analysis platforms and computational methods for analyzing genomic data.

Clinical Informatics:

Michael Cantor and Dadong Li

Contribution: All authors contributed to the clinical informatics of the project

Translational Genetics:

Niek Verweij, Jonas Nielsen, Tanima De and Manuel A. R. Ferreira

Contribution: All authors contributed to the review process for the final version of the manuscript.

Research Program Management

Marcus B. Jones, Jason Mighty and Lyndon J. Mitnaul

Contribution: All authors contributed to the management and coordination of all research activities, planning and execution. All authors contributed to the review process for the final version of the manuscript.

## 2. Supplementary Methods

### Whole exome sequencing dataset

*Whole exome sequencing (WES)*

Exomes were captured with the IDT xGen Exome Research Panel v1.0 including supplemental probes. The basic design targets 39Mbp of the human genome (19,396 genes). Multiplexed samples were sequenced with dual-indexed 75x75bp paired-end reads on the Illumina NovaSeq 6000 platform using S2 (initial 50k samples) and S4 flow cells (all subsequent samples). In each sample and among targeted bases, coverage exceeds 20X at 95% of sites on average. More information is available on the UK Biobank website (https://biobank.ctsu.ox.ac.uk/showcase/label.cgi?id=170).

*Variant calling for the OQFE dataset*

In the present analysis, we used the pVCF files from the OQFE dataset[1]. Briefly, all reads were duplicate marked and aligned to genome build GRCh38 in an alt-aware manner as described in the Functional Equivalence protocol[2]. Variants were called per-sample using DeepVariant, after which individual level VCF files were combined and joint-genotyped using GLnexus[3]. More information is available on the UK Biobank website (https://biobank.ctsu.ox.ac.uk/showcase/label.cgi?id=170).

### Quality control

In addition to any quality-control that was performed centrally, we applied extensive additional genotype, variant and sample quality-control procedures to ensure a high-quality dataset for analyses. To this end, we utilized the OQFE WES pVCF files provided by the UK Biobank, which contained calls for 200,643 sequenced samples.

*Genotype quality control*

We applied genotype refinement to the raw genotype calls in the pVCF files using Hail. We first split multi-allelic sites to represent separate bi-allelic sites. All calls that did not pass the following hard filters were then set to no-call in our analysis:

- For homozygous reference calls: Genotype Quality < 20; Genotype Depth < 10; Genotype Depth > 200
- For heterozygous calls: (A1 Depth + A2 Depth)/Total Depth < 0.9; A2 Depth/Total Depth < 0.2; Genotype likelihood[ref/ref] < 20; Genotype Depth < 10; Genotype Depth > 200
- For homozygous alternative calls: (A1 Depth + A2 Depth)/Total Depth < 0.9; A2 Depth/Total Depth < 0.9; Genotype likelihood[ref/ref] < 20; Genotype Depth < 10; Genotype Depth > 200

These filters removed 9% of the 3,573,574,459,423 raw genotype calls leaving 3,214,727,581,104 genotype calls across 17,981,897 variant sites and 200,643 samples.

*Variant quality control*

We then performed variant level filters. We removed variants that failed the following filters:

- Call rate of < 90% (restricting to males for Y chromosomal markers) (N= 4,023,284)
- Failed a liberal Hardy-Weinberg Equilibrium test (HWE) at $P < 10^{-15}$ among unrelated samples (not applied to Y chromosomal markers) (N=136,869)
- Present in Ensembl low-complexity regions (N=748,116)
- Monomorphic in the final dataset (N=55,614)

After performing these variant filters, 13,003,057 variants remained of which 12,756,075 were autosomal.

*High-quality variants for sample quality control and relationship inference*

To perform sample level quality control and kinship inference, we defined three subsets of genetic variants that were independent and of very high-quality:

- 'High-quality independent autosomal variants subset' with MAF > 0.1%, missingness < 1%, HWE $P > 10^{-6}$ and two rounds of pruning using *--indep-pairwise 200 100 0.1* and *--indep-pairwise 200 100 0.05* in PLINK[4] (81,121 variants).
- 'WES-vs-array independent autosomal variants subset' with MAF > 0.1%, missingness < 1% and HWE $P > 10^{-6}$ in both the WES dataset and in the genotyping array data provided by the UK Biobank[5] (among participants who had both available). We further removed indels and ambiguous SNPs and performed two rounds of pruning (24,207 variants).
- 'High quality independent X-chromosomal subset' with missingness < 1%, HWE $P > 10^{-6}$, not within pseudo-autosomal regions, and two rounds of pruning.

*Sample quality control*

We computed a number of quality metrics to identify bad-quality or duplicated samples. We first used KING[6] (version 2.2.5) to calculate pairwise heterozygote concordance rates for each pair of samples, using the high-quality independent autosomal markers. Then we used the high-quality autosomal variants present in both WES and array datasets to compute per-sample heterozygote concordance rates between WES calls and genotyping array calls. We inferred the genetic sex of each participants with the *--check-sex* option in PLINK, using the high-quality independent X-chromosomal markers. We set any sample with F > 0.8 to male, while samples with F < 0.5 were set to female. Finally, using all ~12.7M autosomal WES variants, we computed a number of additional metrics including sample call rate, transition/transversion ratio (Ti/Tv), heterozygote/homozygote ratio (Het/Hom), SNV/indel ratio (SNV/indel) and the number of singletons. After computing these metrics, we excluded participants based on the following criteria:

- Decided to revoke their consent (N=13)
- Sample duplicates based on heterozygote concordance rates > 0.8 (N=0) (27 putative genetic duplicates could be resolved as monozygotic twins and were not removed)
- Samples with blatant discordance between self-reported and genetically inferred sex (N=80)
- Discordance between WES and array calls with heterozygote concordance rates < 0.8 (N=0)
- Call rate < 90% (N=1)
- Samples further than 8 standard deviations from the mean for Ti/Tv (n=0), Het/Hom (N=100), SNV/indel (N=1) and number of singletons (N=111)

After applying these filters 200,337 samples remained for analysis.

**Relationship inference, kinship matrix and principal component analysis**

*Kinship inference and kinship matrix*

We used the KING-robust algorithm to compute pairwise kinship estimates for all samples in the dataset (using the high-quality independent autosomal variants). We then retained all information on pairs estimated to be genetically related to one another at 3$^{rd}$ degree or closer (kinship coefficient >=0.0442). We used this data to construct a sparse kinship matrix in which all relationships with kinship coefficient <0.0442 were set to 0. Finally, we scaled the values in this matrix so it had a diagonal of 1 (as opposed to 0.5 on the KING kinship scale).

*Unrelated subset*

We defined an unrelated subset of the WES cohort, where no relationships with kinship coefficient >=0.0442 remained, a threshold that excludes any individuals related at 3$^{rd}$ degree or closer. To maximize the sample size of this unrelated subset, we first iteratively removed individuals related to multiple other individuals until none remained. We then removed one sample from each remaining pair at random, leaving 185,990 unrelated samples.

*Principal component analysis*

PCAir[7] (from GENESIS version 2.18.0) was used to calculate the top 20 ancestral principal components (using the high-quality independent autosomal variants), while implementing a randomized algorithm[8] for computational efficiency. We performed this analysis among the unrelated subset of the cohort, after which the remaining samples were projected onto the PCs.

**Variant annotation for missense variants**

Missense variants annotated from VEP incorporated 30 in-silico prediction tools from the dbNSFP database (version 4.1a.) These tools included qualitative prediction algorithms (SIFT, SIFT4G, Polyphen2 HDIV, Polyphen2 HVAR, LRT, MutationTaster, FATHMM, PROVEAN, MetaSVM, MetaLR , MCAP, PrimateAI, DEOGEN2, BayesDel addAF, BayesDel noAF, ClinPred, LIST-S2, fathmm-MKL coding, fathmm-XF coding, MutationAssessor, and Aloft) and quantitative algorithms (VEST4, REVEL, MutPred, MVP, MPC, DANN, CADD, Eigen, and Eigen-PC). When the qualitative prediction tools (except for MutationAssessor and Aloft) indicated "D" for a variant, the variant gained one score from each algorithm. An indicator for a deleterious variant of MutationAssessor was "H" and of Aloft was "R" or "D" with high confidence. For the quantitative algorithms, when the variant indicators were higher than 90% of predicted variants in the entire dataset, a variant gained one score from each quantitative algorithm. Then, if a variant was annotated with more than seven prediction tools (over 20% out of the 30 tools), and the proportion of the deleterious score (total gained score / # none missing prediction tools) was greater than or equal to 0.9, we included the variant in the gene-based analyses.

**Evaluation of test statistic inflation in exome-wide gene-based testing**

To inspect the calibration of test statistics in our analyses, we visually inspected quantile-quantile (QQ) plots across all performed tests for binary traits, and across all performed tests for quantitative traits. To evaluate the effect of the minimum carrier count we employed (≥20 rare variant carriers), we further made QQ plots for all test with ≥50, and all tests with ≥200 rare variant carriers. Then we inspected per-trait QQ plots and computed per-trait λ values, representing a statistic of inflation where a value of 1 indicates perfect calibration of *P*-values. For quantitative traits, we computed λ at the median (λ[median]), as is conventional. For binary traits, the Saddle Point Approximation was only applied to tests reaching $P<0.05$ in an initial regular score test. For this reason, λ(median) may not accurately represent test statistic inflation at the tails of the distribution. We therefore computed λ values for binary traits at the tail of the test statistic distribution, by comparing empirical values at the 95$^{th}$ quantile to the expected value at the 95$^{th}$ quantile (λ[q0.95]).

**Analysis of rare synonymous variants**

For any trait showing unexplained test statistic inflation, we analyzed rare synonymous variants. Synonymous variants are generally expected to have no protein consequence, and therefore represent a class of genetic variation that should produce a null distribution. As with the predicted-deleterious variants, we pooled rare synonymous variants variant by gene and performed a collapsing test. Variants were considered rare if they had MAF<0.1% in the UK Biobank WES dataset and MAF<0.1% in five major gnomAD[9] populations.

**Analysis of common variation near rare variant signals in the UK Biobank**

To identify common variant associations near the identified rare variant signals, we ran common variant association analyses in the genomic region 500KB downstream and upstream of the identified gene. To this end, we utilized the UK Biobank version 3 imputed data. Details on genotyping and quality-control have been described previously[5]. Briefly, samples were genotyped using Affymetrix UK biobank Axiom (450,000 samples) and Affymetrix UK BiLEVE axiom (50,000 samples) arrays. Genetic data were then imputed to the Haplotype Reference Consortium panel and UK10K + 1000 Genomes panels. For the common variant association analyses, we removed samples that were outliers for heterozygosity or missingness, samples with putative sex

chromosome aneuploidy, samples with a mismatch between self-reported and genetically inferred sex, samples not included in the central kinship inference, and samples who had revoked their consent. Imputed variants with MAF<0.5% and INFO<0.3 were removed. We ran two-sided common variant association tests using PLINK2[4]. Logistic regression was used for binary phenotypes and linear regression for continuous traits. We analyzed all unrelated UK Biobank individuals with imputed data and relevant phenotypic data available. We adjusted for age, sex, genotyping array and associated ancestral principal components ($P$<0.05). Common variants with $P<1x10^{-5}$ were considered significant.

**Common variant results from the Type 2 Diabetes Portal (T2DKP)**

For genes in which we identified novel rare variant associations for metabolic and anthropometric traits, we aimed to find additional evidence for the role of these genes using publicly-available common variant results from the T2DKP[10]. We used gene-based common variant results downloaded on the 7th of December 2020, displayed in **Supplementary Table 11**. Gene-based results were based on single variant summary statistics from many large-scale common variant GWAS. In short, the portal first filters summary statistics to include only biallelic markers with no missing data, and then separates variants by frequency (common vs rare) and by ancestry. Then, it meta-analyses GWAS results for common variants using METAL[11] (with OVERLAP ON) in a ancestry-specific manner, after which it performs a trans-ancestry meta-analysis using METAL (with OVELAP OFF). Gene-based common variant analyses were subsequently performed using the Multi-marker Analysis of GenoMic Annotation method (MAGMA)[12]. We further identified index single variants using the 'explore region' option for a given gene; the most significant single variant in a gene region for a given phenotype were extracted from the T2DKP data on the 7th of June 2021, displayed in **Supplementary Table 12**.

**GTEx expression-QTL and splice-QTL data for common variants**

For each index single variant from the T2DKP mentioned above, we leveraged data from GTEx to identify significant expression-QTL and splice-QTL associations. For a few phenotypes, no data in the T2DKP was available; in these cases, we used the index variants from our imputed common variant analyses in the UK Biobank (e.g. supraventricular tachycardia and *TTN*). We extracted expression-QTL and splice-QTL data for index variants and the relevant gene from the GTEx version 8 dataset (https://gtexportal.org/home/), on the 7th of June 2021. The dataset consists of RNA-sequencing and whole-genome sequencing data from 838 donors after previously described quality-control[13]; 49 tissues or cell lines had at least 70 individuals with both data sources available (15,201 total samples) for expression-QTL and splice-QTL analysis. We determined that a variant was a significant expression-QTL for the given gene if i) the expression-QTL reached tissue-specific FDR5%, as described previously[13] and ii) had Bonferroni-corrected $P < 7.3x10^{-5}$ = 0.05 / (14 variants x 49 tissues) in our analysis. Splice-QTLs were determined to be significant if i) the splice-QTL reached tissue-specific FDR5%, as described previously[13] and ii) had Bonferroni-corrected $P < 1.6x10^{-6}$ = 0.05 / (629 introns x 49 tissues) in our analysis. Results for this lookup are displayed in **Supplementary Table 12**.

**Clinical variants from the ClinVar database**

To identify pathogenic rare variants, we used the ClinVar database. We downloaded the ClinVar dataset on 11/2020. Variants that were not submitted by clinical testing labs or which were evaluated before 2015 were excluded from our analyses. We used the clinical significance interpretation at the most recent submission. The clinical significance interpretation included Pathogenic, Likely-Pathogenic, Likely-Benign, Benign, Variant of Uncertain Significance, and Conflicting data from submitters; we only used variants with the Pathogenic or Likely-Pathogenic classification in the present study.

***TTN* exons highly expressed in left ventricle tissue**

Previous work described that distinguishing highly expressed *TTN* exons in heart tissues is important to understand phenotypic presentation[14,15]. As post-hoc analyses, we performed association tests between

deleterious variant in highly expressed (Percentage Spliced-In [PSI] ≥ 90%) in left ventricular tissue[14] and cardiac traits using the same model implemented in our primary analyses.

## 3. Supplementary Results and Discussion

### Evaluation of inflation in gene-based analyses

QQ plots for *P*-values from all performed tests in the discovery phase (all quantitative and all binary) did not show any inflation (**Supplementary Figure 2**). We also made QQ plots restricting to tests with at least 50 variant carriers and tests with at least 200 rare variant carriers (**Supplementary Figure 2**)**.** QQ plots showed a similar distribution of *P*-values without clear inflation. We then inspected QQ plots for individual traits (**Supplementary Figures 3-4**). Most traits did not show evidence of inflation ($\lambda<1.1$); however for three traits, height, weight and QTc, lambda values were consistent with moderate inflation ($1.1\leq\lambda_{GC}<1.25$). Indeed, height and weight had visually inflated distributions of *P*-values. Such inflation could be due to biases such as population stratification, or alternatively due to a high degree of polygenicity. To distinguish between these causes, we analyzed rare synonymous variants for these traits. Seeing as most synonymous variants are expected to have no protein consequence, such an analysis should yield a null distribution. We found that rare synonymous variants indeed yielded a distribution of *P*-values consistent with the null ($\lambda_{GC}<1.05$) for each traits (**Supplementary Figure 5**), implying that a large proportion of the observed inflation was due to polygenicity rather than bias.

### Associations between cardiac phenotypes and variants in *TTN* exons highly expressed in the heart

Concordant with our prior knowledge *TTN* associations with heart failure, atrial fibrillation, dilated cardiomyopathy, left ventricle ejection fraction and left ventricular end systolic volume strengthened after restricting to variants in cardiac expressed exons. Supraventricular tachycardia ($P = 3.0\times10^{-12}$), ventricular arrhythmia ($P = 2.6\times10^{-10}$), and mitral valve disease ($P = 5.4\times10^{-15}$) also showed markedly stronger associations when restricting to cardiac exons of *TTN*. Furthermore, implantable cardioverter defibrillator ($P = 6.6\times10^{-9}$), tricuspid valve disease ($P = 9.7\times10^{-7}$), RR interval ($P = 2.6\times10^{-6}$), Pulse rate ($P = 1.1\times10^{-25}$) and LVESVi ($P = 1.8\times10^{-7}$) were significantly associated with variants in cardiac exons of *TTN*.

### Common variants near genes with novel rare variant associations

Among our novel associations were 3 associations for rare variants in *GIGYF1*, namely for increased risk of type 2 diabetes, elevated glucose levels and lower low-density lipoprotein levels. In accordance, common variants near *GIGYF1* were associated with all these traits (**Supplementary Table 11**). The top common variants for each of these traits in the *GIGYF1* locus are expression-QTLs for *GIGYF1* in many tissues (**Supplementary Table 12**), including many relevant tissues such as adipose tissue, pancreas, skeletal muscle, thyroid and pituitary, as well as many other brain and gastro-intestinal tissues. The alleles associated with lower *GIGYF1* expression were consistently associated with increased risk of diabetes, higher glucose and lower low-density lipoprotein levels across tissues, in strong concordance with the observed LOF associations. These results suggest that higher *GIGYF1* levels may be protective for diabetes. *CCAR2* rare variants were associated with increased risk of diabetes, and common variants near the locus were as well (**Supplementary Table 11**). The top *CCAR2* common variant was a significant expression-QTL for *CCAR2* across many tissues, including adipose tissue, skeletal muscle, pancreas, thyroid and multiple brain and gastro-intestinal tissues (**Supplementary Table 12**). Generally, the alleles associated with higher *CCAR2* expression were associated with higher risk of diabetes, which is not directly consistent with the observed LOF associations, although the sign was flipped in certain tissues such as fibroblasts.

Rare variants in *TTN* were novelly associated with mitral valve disease and supraventricular tachycardia. A common variant near *TTN* was also found to be associated with supraventricular tachycardia (rs10167882, $P=2.1\times10^{-6}$, OR 1.11; **Supplementary Table 12**). This variant was not found to be a significant expression-QTL or splice-QTL for *TTN*, although it is in LD with a missense variant that also shows evidence of

association with supraventricular tachycardia as well (p.Gln8542His, *P*=0.0015, OR 1.23; **Supplementary Table 12**).

Rare variants in *NR1H3* were associated with high-density lipoprotein in our primary analysis, and a common variant association was also found at this locus (**Supplementary Table 11**). The top common variant in this locus was an expression-QTL for *NR1H3*, with the alleles associated with higher high-density lipoprotein being associated with increased *NR1H3* expression in some tissues (for example subcutaneous adipose tissue) and decreased expression in others (whole blood, brain cortex) (**Supplementary Table 12**). The top common variant was also a significant splice-QTL for *NR1H3* across many tissues including adipose tissue, with consistent tissue effects, and was also in LD with an *NR1H3* missense variant (p.Ala101Val, $P=1.9\text{x}10^{-21}$) (**Supplementary Table 12**).

Among our novel rare variant associations were 7 associations for height, namely *DTL*, *PIEZO1*, *SCUBE3*, *ANGPTL2*, *PAPPA*, *IRS1* and *ZFAT.* All of these genes are supported by significant nearby common variant associations (**Supplementary 11**). For *IRS1*, we found that the top common variant had two splice-QTL associations with *IRS1*: one in fibroblasts and thyroid, and another in subcutaneous adipose tissue (**Supplementary Table 12**). For *PAPPA*, we found that the top common variant was in LD with a *PAPPA* missense variant (p.Ser1224Tyr). Finally, for *SCUBE3*, we found that the top common variant was a suggestive (*P*=0.00019) expression-QTL for *SCUBE3* in fibroblasts, with the allele associated with lower *SCUBE3* expression being associated with shorter stature, consistent with the observed LOF association. The relative absence of additional expression-QTL and splice-QTL data for the remaining common variant height loci might be a reflection of the adult population in GTEx; relevant expression-QTLs for height may be predominantly developmental and possibly not present in adult tissue.

**Penetrance of predicted-deleterious and pathogenic variants in the UK Biobank**

In our primary analyses, 10 genes were significantly associated (Q-value < 0.01) with increased risk of a disease or medical condition. For those 10 genes, 3371 participants (1.6% of the sample) carried predicted-deleterious variants (LOF and predicted-deleterious missense variants). Among 3371 carriers, 621 (18.4% penetrance) developed at least one medical condition. When we liberalize our significant threshold to FDR Q-value 0.05, there were 15 genes associated with at least one medical condition. We found 3762 participants (1.9% of the sample) who carried deleterious variants; meanwhile 693 (18.4% penetrance) developed an associated disease. The penetrance of respective genes and traits are illustrated in **Supplementary Figure 11**. The highest penetrance was 71% [95%CI 61-79%] from *LDLR* for hypercholesterolemia. *PKD1* mutations were associated with 47% penetrance for chronic kidney disease [95%CI 33-62%]. *PKD1* pathogenic mutations are known for causing highly-penetrant autosomal dominant polycystic kidney disease, with end stage kidney disease reached at around 58 years[16]. However, a higher-than-expected frequency of *PKD1* mutations in healthy sequenced populations has recently been described, suggesting incomplete penetrance[17]. We note, however, that *PKD1* has many pseudo-genes which may complicate read-mapping, and Sanger sequencing validation is often performed in clinical settings to confirm *PKD1* variants. Despite this fact, previous studies have mainly shown decreased sensitivity when utilizing next-generation sequencing; specificity ranges from 90-100% when stringent QC filters are applied[18-20]. Still, we cannot exclude the possibility of some alignment issues, which may downward bias penetrance estimates for this gene.

The penetrance of putatively pathogenic variants in genes included in our panel analysis (*InVitae Cardiomyopathy and Arrhythmia* panel, *InVitae hypercholesterolemia panel* and *InVitae Monogenic Diabetes* panel) are shown in **Supplementary Figure 13**. The penetrance of cardiovascular disease variants was generally modest (**Supplementary Table 10**). Of *TTNtv* carriers, 16% [95%CI 14-19%] had diagnoses of atrial fibrillation, 9.6% [95%CI 7.9-12%] of heart failure, 4.0% [95%CI 2.8-5.6%] of dilated cardiomyopathy and 3.8%

[95%CI 2.6-5.3%] of ventricular arrhythmia (**Supplementary Table 10**), considerably lower than the incidence of these diseases in previous family-member based analyses[21,22], although for cardiomyopathy and atrial fibrillation estimates were not dissimilar to genome-first estimates from the Geisinger Health System[23]. Penetrance of *MYBPC3* and *MYH7* putatively pathogenic variants for hypertrophic cardiomyopathy was 7.0% [95%CI 4.1-11%] and 4.8% [95%CI 2.9-7.0%], respectively (**Supplementary Table 10**). *MYBPC3* LOFs were associated with 9.7% [95%CI 4.5,18%] penetrance. Relative-based analyses have frequently yielded estimates over 30% for sarcomere mutations[24-27], although we note that our OR estimate for *MYBPC3* LOFs is very consistent with a previous case-control study[28]. Similarly, family-member analyses have reported 40% incidence of arrhythmogenic cardiomyopathy/dysplasia for pathogenic desmosome mutations[29], yet we find that fewer than 5% of *PKP2* and *DSP* variant carriers have diagnoses of dilated cardiomyopathy or ventricular arrhythmia; fewer than 12% of carriers had atrial fibrillation (**Supplementary Tables 10** and **15**).

The penetrance estimates of *GCK* and *HNF1A* putatively pathogenic variants for type 2 diabetes were large at 64% [95%CI 49-78%] and 45% [95%CI 26-64%], respectively, with an age dependent penetrance (**Supplementary Table 10**). Previous studies have suggested that *HNF1A* mutations have over 90% penetrance for progressive diabetes at 50 years of age[30], while *GCK* mutations are thought to cause a shift in glucose-sensing and mild hyperglycemia from birth[31]. Interestingly, *GCK* LOF mutations - such as those contributing strongly to our signal - are found in MODY patients[32], and rare *GCK* mutations are also enriched in individuals diagnosed with type 2 diabetes[33]. Further population-based assessment seems warranted to determine diabetes-related outcomes, given the conventional knowledge that *GCK* mutations cause hyperglycemia that often does not require medical intervention[31].

Penetrance estimates for significant associations at different cut-offs for age-at-onset are shown in **Supplementary Table 10,** showing an age-dependent probability of diagnosis for most gene-phenotype pairs. We acknowledge that these penetrance estimates are based on age-at-diagnosis, which may be inaccurate for diseases defined at UK Biobank visits. However, for age-specific penetrance estimates, we did not include cases defined at baseline for this reason; we further found that electronic health records were the most important source of data for many phenotypes (**Supplementary Table 2**). This should be considered when interpreting the age-stratified penetrance estimates, as true age-at-onset may be earlier than age-at-diagnosis based on ICD codes. In addition, by excluding cases defined by self-report at baseline, some individuals with early-onset disease may have been excluded for age-stratified analyses. Despite these limitations, these analyses highlight how age is an important factor in disease presentation in carriers of pathogenic variation.

Overall, our penetrance results highlight - from a genome-first perspective - substantially lower penetrance for pathogenic variation than previously reported from family-based analyses. This finding is consistent with previous analyses in the UK Biobank that utilized well-genotyped likely-pathogenic rare variants from the genotyping array[34]. There are various factors that should be taken into account when interpreting population-based penetrance estimates. First, some survivor and ascertainment bias are to be expected in our relatively healthy middle-aged population-based cohort, which may bias penetrance estimates downwards. Furthermore, it is possible that certain putatively pathogenic variants included in our analysis are not truly pathogenic variants; for example, the 'likely pathogenic' variants from ClinVar may include some non-pathogenic alleles, and certain LOF variants may not be truly LOF. To mitigate these issues, we only included ClinVar variants reported from 2015 onwards (which should therefore conform to stringent guidelines for pathogenicity assertions) and we used LOFTEE to filter out as many low-confidence or dubious LOF variants as possible. Third, for many of the diseases, cases were defined primarily by ICD codes, which may downward bias penetrance estimates for diseases that can go undiagnosed or that are diagnosed outside of the hospital (e.g. diabetes, dyslipidemias, chronic kidney disease). Therefore, our estimates may reflect more severe symptomatic cases, while not including subclinical and mildly symptomatic disease. However, given strikingly

high penetrance estimates for pathogenic variation in hypercholesterolemia and diabetes genes (>60% for *LDLR* and *GCK*), this effect generally appears not to be large. On the other hand, the high penetrance estimates from family-member analyses are likely biased upwards. First, since many family-member based analyses are based on clinically ascertained index cases with severe disease, such analyses are strongly biased towards families prone to more severe disease and higher disease penetrance. Second, in-depth phenotyping in such studies may over-diagnose disease even though clinical symptoms may never have arisen. In sum, true penetrance estimates likely lie somewhere in between population-based estimates and family-based/clinical cohort estimates.

**Yield of putatively pathogenic variants among disease cases**

The yield of rare putatively pathogenic variants was generally low among disease cases. Among heart failure and atrial fibrillation cases, the yield of associated pathogenic variants was ~1.5% and ~1.1%, respectively. For hypertrophic and dilated cardiomyopathy, the yield of associated putatively pathogenic variants was ~11.0% and ~10.1%, respectively (**Supplementary Table 17 and Supplementary Figure 14**). It should be noted that rare variant yield in this case only represents the yield of LOFs, known likely pathogenic variants and known pathogenic variants in genes showing evidence of association at $P<0.005$. As such, this yield is a conservative lower-bound estimate that should rise as more genes are included and more non-truncating pathogenic variants are discovered.

## Supplementary Tables

**Supplementary Tables 1-17** can be found in the **Supplementary Excel File.**

## Supplemental Figures

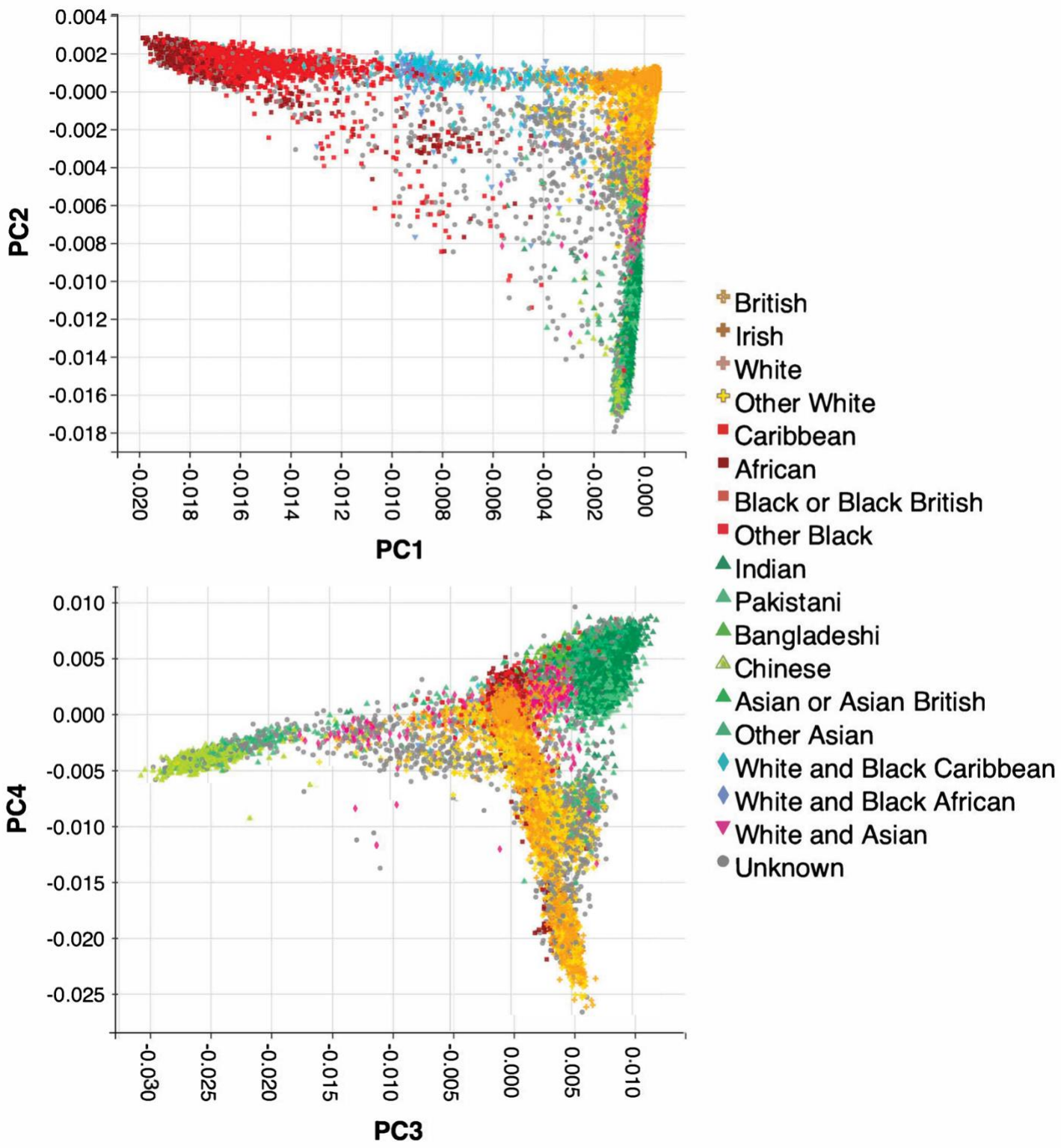


**Supplementary Figure 1. Principal component analysis and self-reported ancestries for UK Biobank WES samples.** Samples are plotted for PC1-4, and self-reported ancestries are highlighted. The principal components stratify samples from different major ancestral groups.

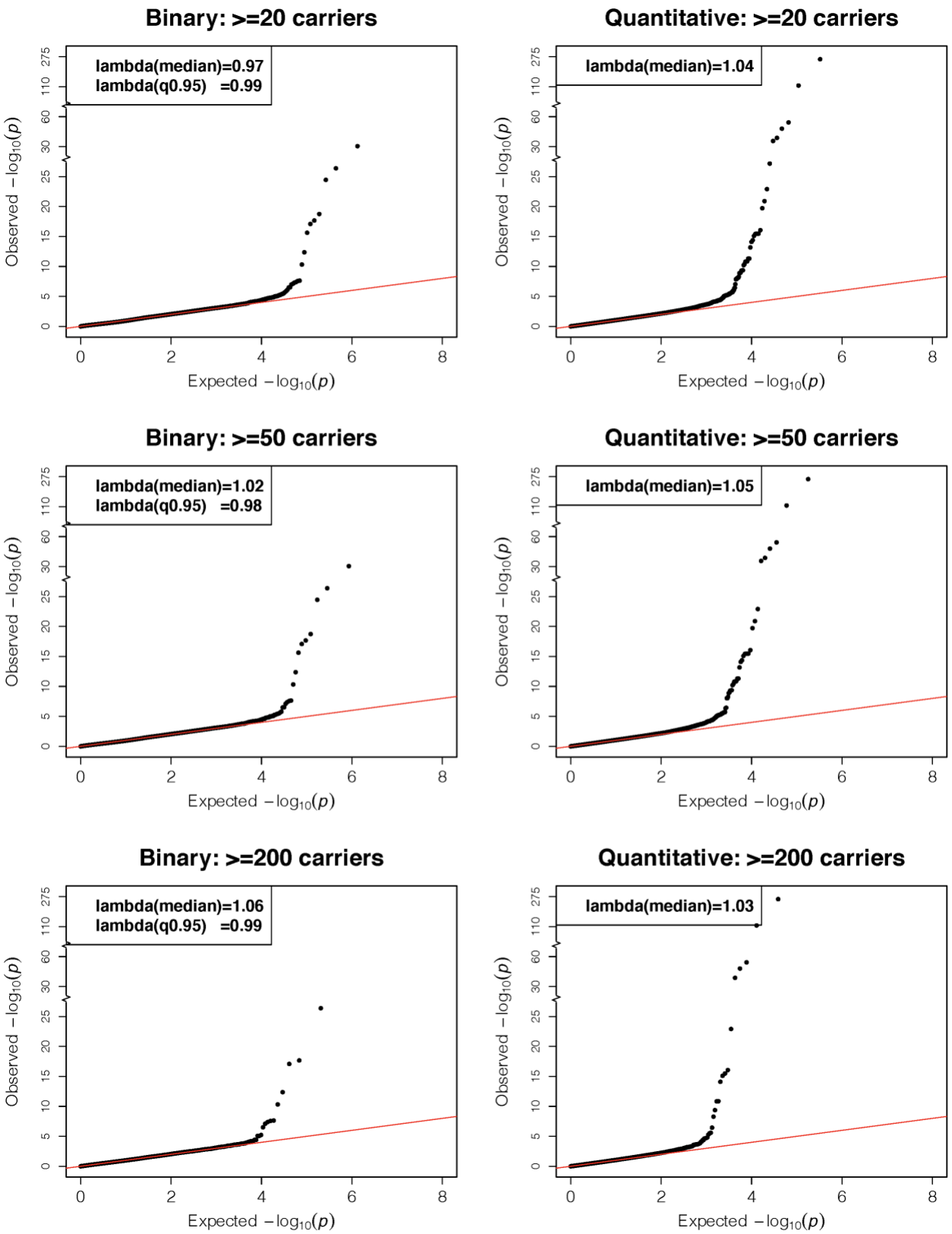


**Supplementary Figure 2: Quantile-quantile plots for exome-wide gene-based tests across all binary and all quantitative phenotypes.** The y-axis represents the observed –log10 *P*-values across all tests, while the x-axis represents the expected under the null-hypothesis. *P*-values were obtained from score tests in linear mixed effects models (quantitative traits) or saddle point approximation in logistic mixed effects models (binary traits), adjusting for sex, age, sequencing batch, MRI serial number (for MRI traits), associated principal

components (PCs) and a sparse kinship matrix. *P*-values shown are two-sided and unadjusted for multiple testing, The left panels show the results for binary traits (for tests with >=20 carriers, 50 carriers and 200 carriers), while the right panels show the results for quantitative traits. Across all performed tests, no systemic inflation is observed.

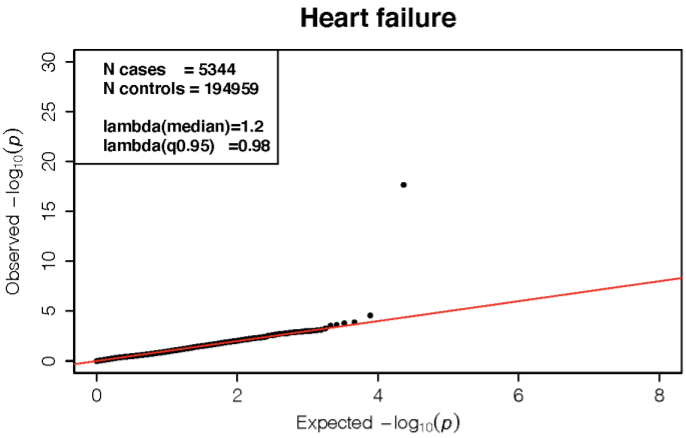
Heart failure
N cases = 5344
N controls = 194959
lambda(median)=1.2
lambda(q0.95) =0.98
Observed $-\log_{10}(p)$
Expected $-\log_{10}(p)$

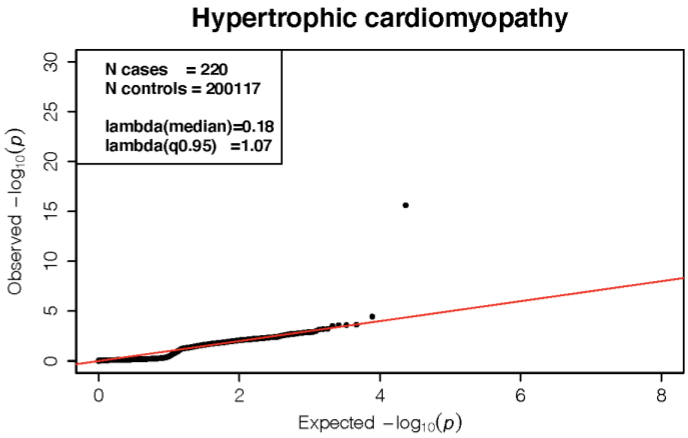
Hypertrophic cardiomyopathy
N cases = 220
N controls = 200117
lambda(median)=0.18
lambda(q0.95) =1.07
Observed $-\log_{10}(p)$
Expected $-\log_{10}(p)$

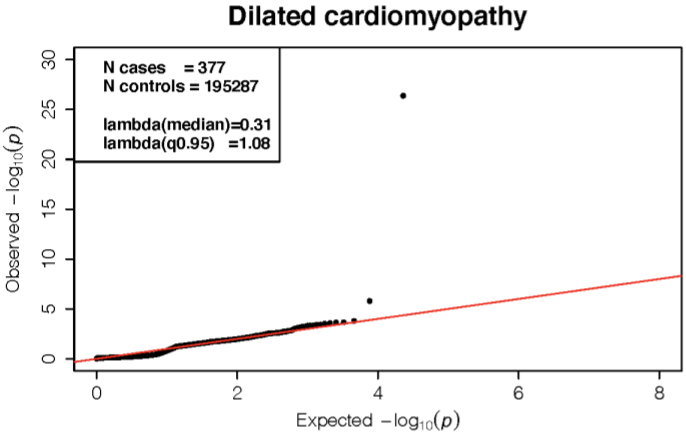
Dilated cardiomyopathy
N cases = 377
N controls = 195287
lambda(median)=0.31
lambda(q0.95) =1.08
Observed $-\log_{10}(p)$
Expected $-\log_{10}(p)$

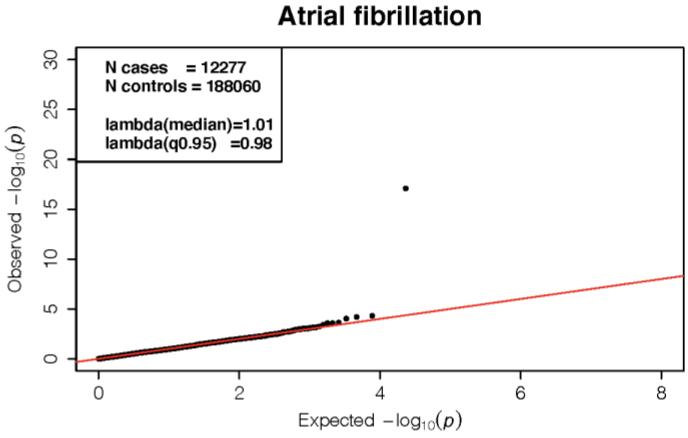
Atrial fibrillation
N cases = 12277
N controls = 188060
lambda(median)=1.01
lambda(q0.95) =0.98
Observed $-\log_{10}(p)$
Expected $-\log_{10}(p)$

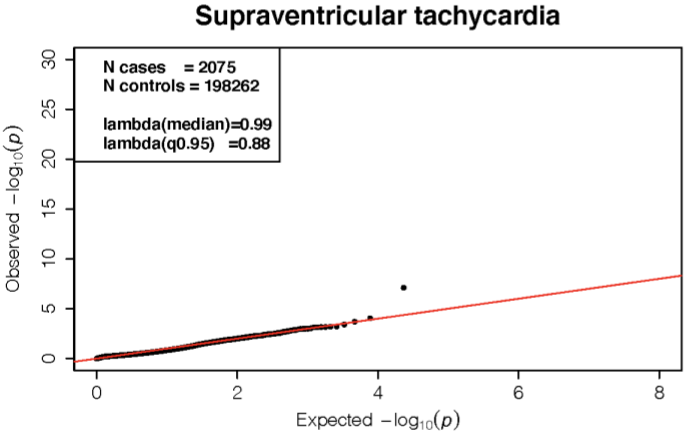
Supraventricular tachycardia
N cases = 2075
N controls = 198262
lambda(median)=0.99
lambda(q0.95) =0.88
Observed $-\log_{10}(p)$
Expected $-\log_{10}(p)$

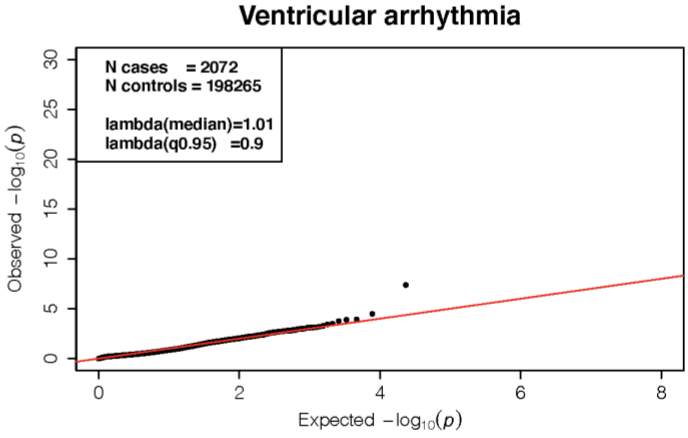
Ventricular arrhythmia
N cases = 2072
N controls = 198265
lambda(median)=1.01
lambda(q0.95) =0.9
Observed $-\log_{10}(p)$
Expected $-\log_{10}(p)$

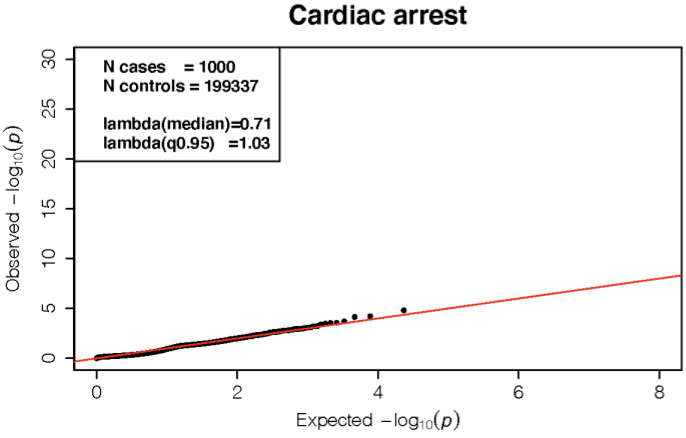
Cardiac arrest
N cases = 1000
N controls = 199337
lambda(median)=0.71
lambda(q0.95) =1.03
Observed $-\log_{10}(p)$
Expected $-\log_{10}(p)$

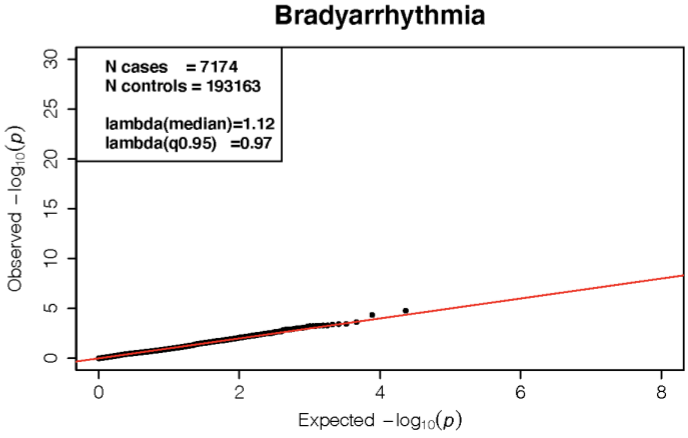
Bradyarrhythmia
N cases = 7174
N controls = 193163
lambda(median)=1.12
lambda(q0.95) =0.97
Observed $-\log_{10}(p)$
Expected $-\log_{10}(p)$

457

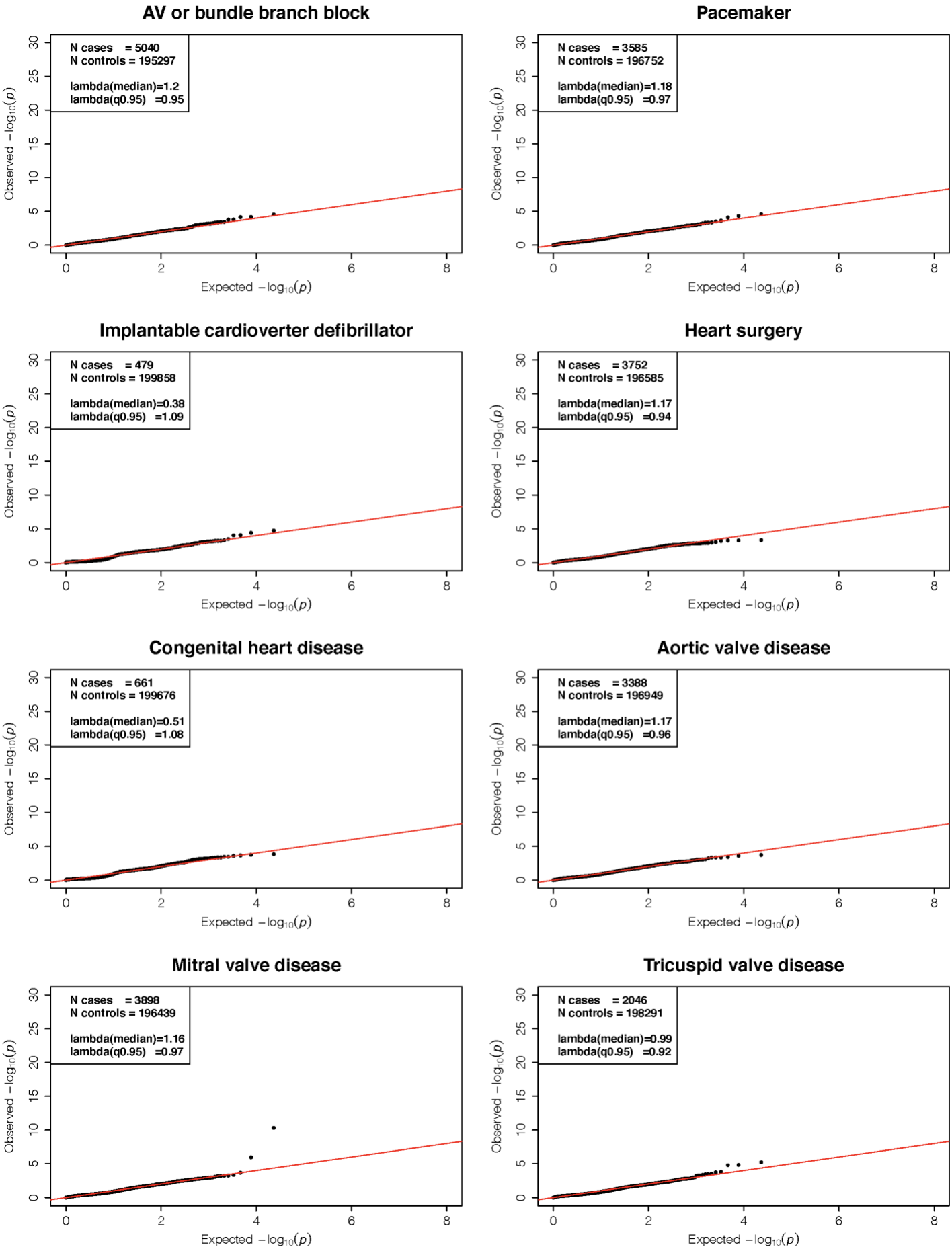
AV or bundle branch block
N cases = 5040
N controls = 195297
lambda(median)=1.2
lambda(q0.95) =0.95
Pacemaker
N cases = 3585
N controls = 196752
lambda(median)=1.18
lambda(q0.95) =0.97
Implantable cardioverter defibrillator
N cases = 479
N controls = 199858
lambda(median)=0.38
lambda(q0.95) =1.09
Heart surgery
N cases = 3752
N controls = 196585
lambda(median)=1.17
lambda(q0.95) =0.94
Congenital heart disease
N cases = 661
N controls = 199676
lambda(median)=0.51
lambda(q0.95) =1.08
Aortic valve disease
N cases = 3388
N controls = 196949
lambda(median)=1.17
lambda(q0.95) =0.96
Mitral valve disease
N cases = 3898
N controls = 196439
lambda(median)=1.16
lambda(q0.95) =0.97
Tricuspid valve disease
N cases = 2046
N controls = 198291
lambda(median)=0.99
lambda(q0.95) =0.92
Observed $-\log_{10}(p)$
Expected $-\log_{10}(p)$

458

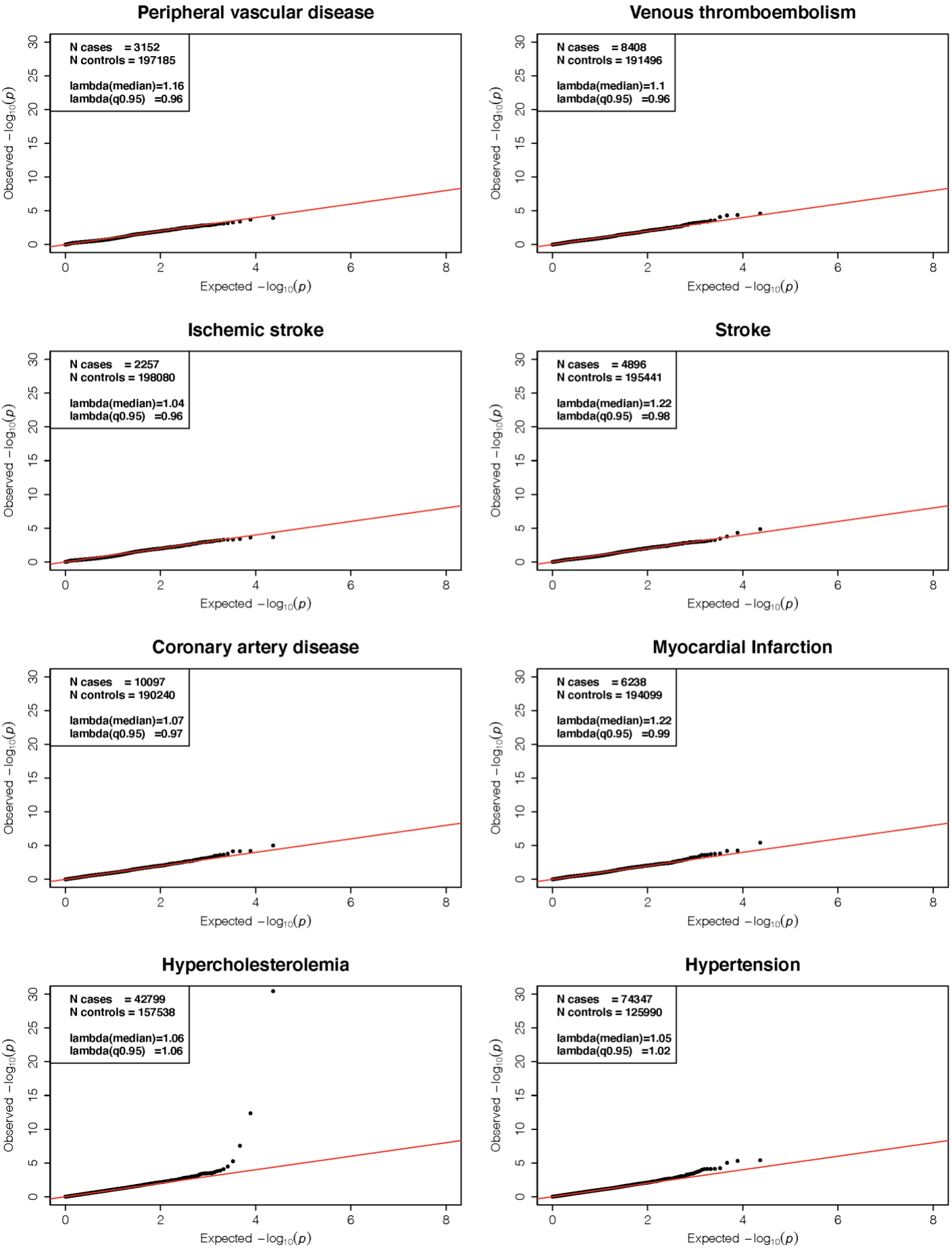
Peripheral vascular disease
N cases = 3152
N controls = 197185
lambda(median)=1.16
lambda(q0.95) =0.96
Venous thromboembolism
N cases = 8408
N controls = 191496
lambda(median)=1.1
lambda(q0.95) =0.96
Ischemic stroke
N cases = 2257
N controls = 198080
lambda(median)=1.04
lambda(q0.95) =0.96
Stroke
N cases = 4896
N controls = 195441
lambda(median)=1.22
lambda(q0.95) =0.98
Coronary artery disease
N cases = 10097
N controls = 190240
lambda(median)=1.07
lambda(q0.95) =0.97
Myocardial Infarction
N cases = 6238
N controls = 194099
lambda(median)=1.22
lambda(q0.95) =0.99
Hypercholesterolemia
N cases = 42799
N controls = 157538
lambda(median)=1.06
lambda(q0.95) =1.06
Hypertension
N cases = 74347
N controls = 125990
lambda(median)=1.05
lambda(q0.95) =1.02
Observed −log10(p)
Expected −log10(p)

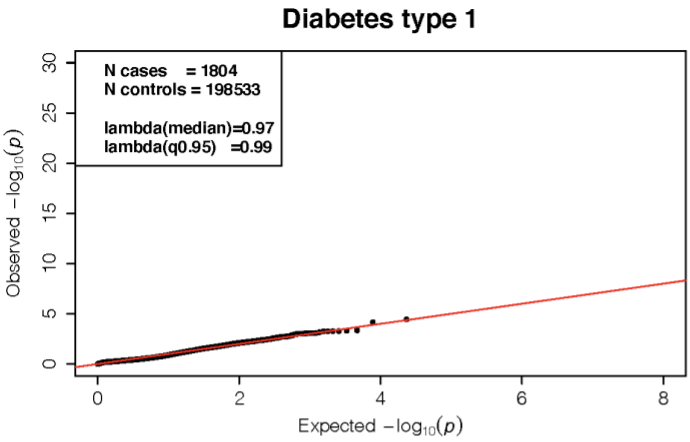
Diabetes type 1
N cases = 1804
N controls = 198533
lambda(median)=0.97
lambda(q0.95) =0.99
Observed −log10(p)
Expected −log10(p)

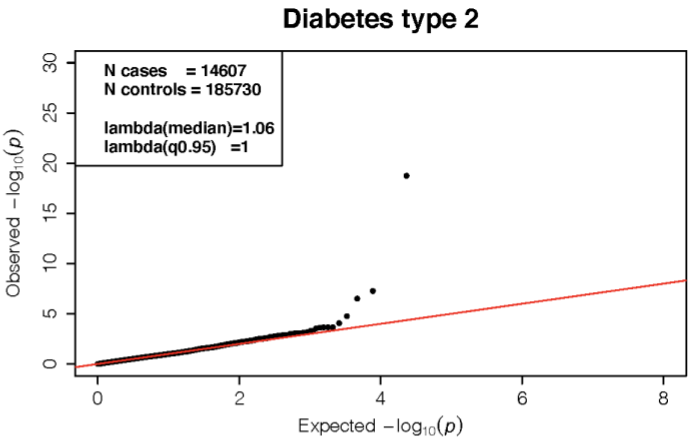
Diabetes type 2
N cases = 14607
N controls = 185730
lambda(median)=1.06
lambda(q0.95) =1
Observed −log10(p)
Expected −log10(p)

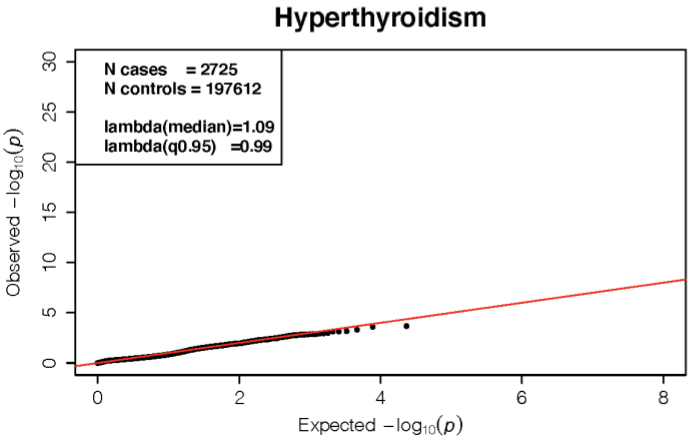
Hyperthyroidism
N cases = 2725
N controls = 197612
lambda(median)=1.09
lambda(q0.95) =0.99
Observed −log10(p)
Expected −log10(p)

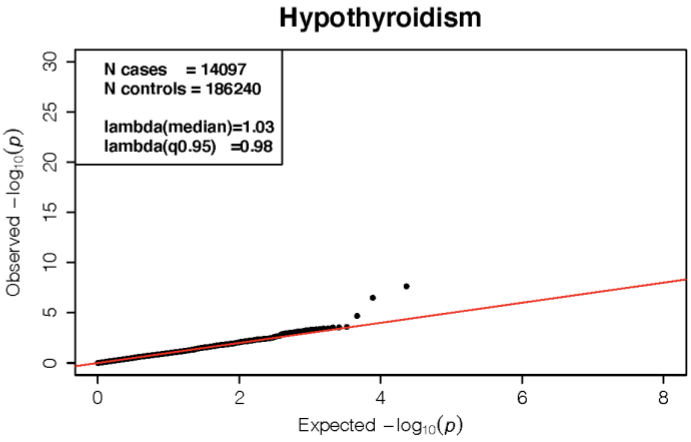
Hypothyroidism
N cases = 14097
N controls = 186240
lambda(median)=1.03
lambda(q0.95) =0.98
Observed −log10(p)
Expected −log10(p)

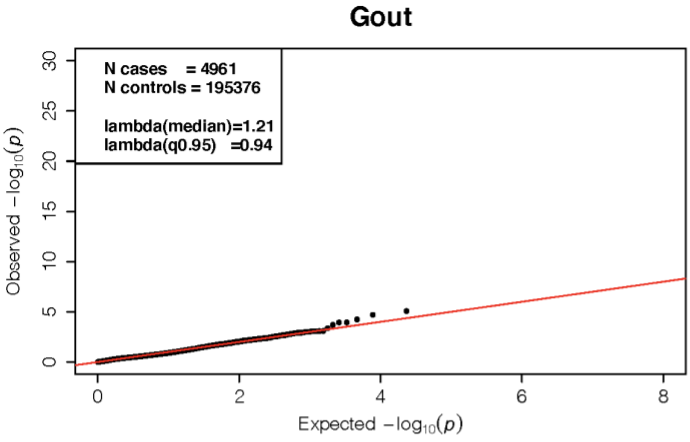
Gout
N cases = 4961
N controls = 195376
lambda(median)=1.21
lambda(q0.95) =0.94
Observed −log10(p)
Expected −log10(p)

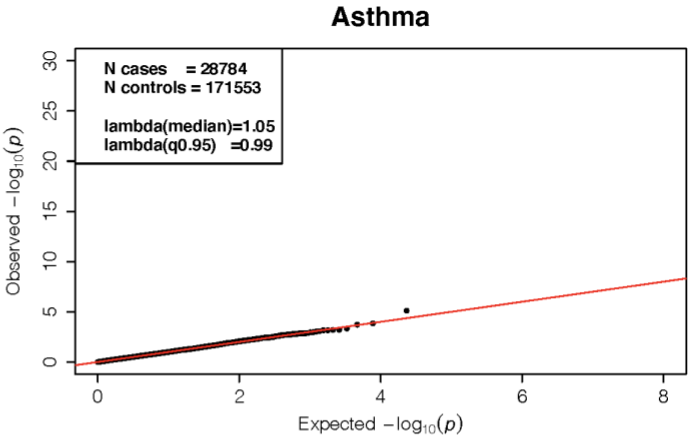
Asthma
N cases = 28784
N controls = 171553
lambda(median)=1.05
lambda(q0.95) =0.99
Observed −log10(p)
Expected −log10(p)

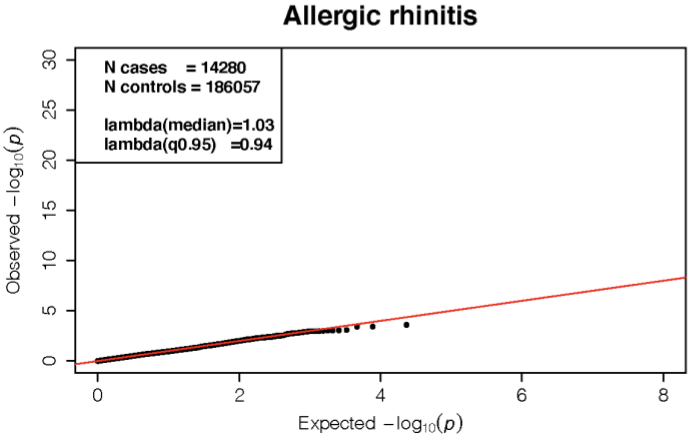
Allergic rhinitis
N cases = 14280
N controls = 186057
lambda(median)=1.03
lambda(q0.95) =0.94
Observed −log10(p)
Expected −log10(p)

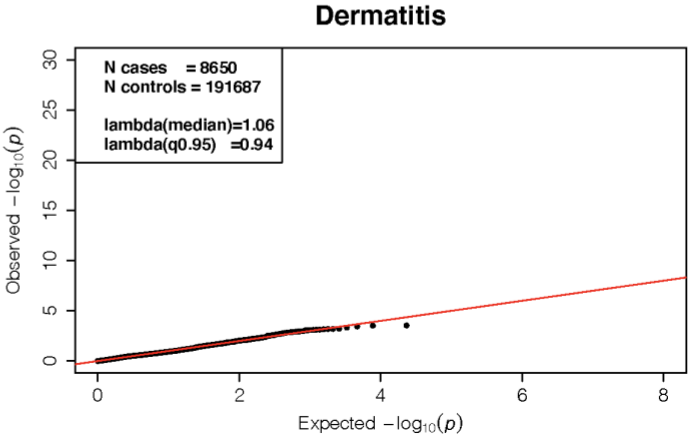
Dermatitis
N cases = 8650
N controls = 191687
lambda(median)=1.06
lambda(q0.95) =0.94
Observed −log10(p)
Expected −log10(p)

460

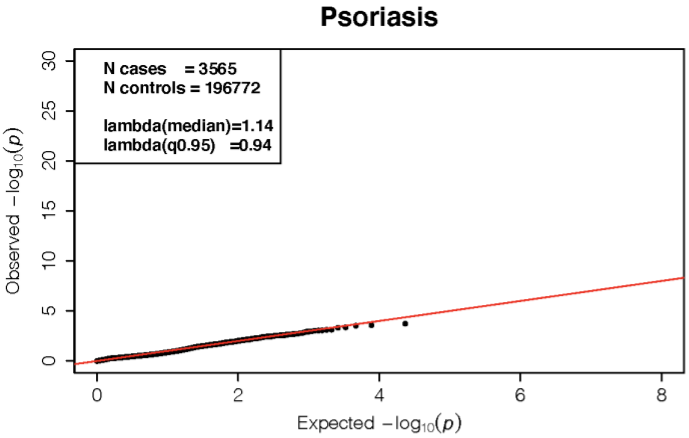
Psoriasis
N cases = 3565
N controls = 196772
lambda(median)=1.14
lambda(q0.95) =0.94
Observed −log10(p)
Expected −log10(p)

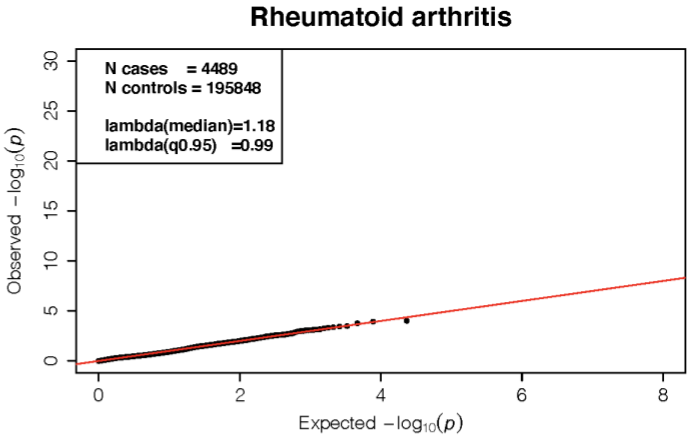
Rheumatoid arthritis
N cases = 4489
N controls = 195848
lambda(median)=1.18
lambda(q0.95) =0.99
Observed −log10(p)
Expected −log10(p)

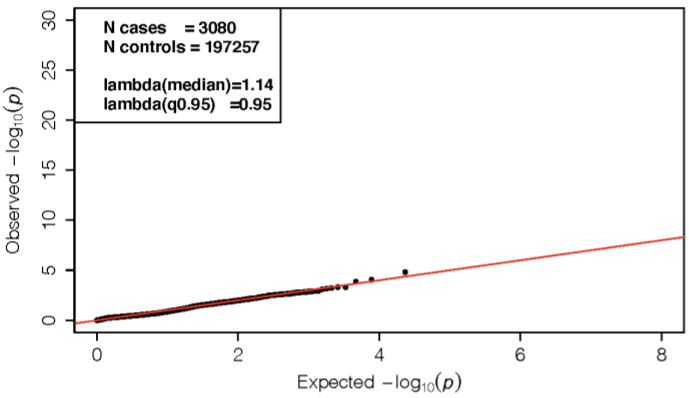
Inflammatory bowel disease
N cases = 3080
N controls = 197257
lambda(median)=1.14
lambda(q0.95) =0.95
Observed −log10(p)
Expected −log10(p)

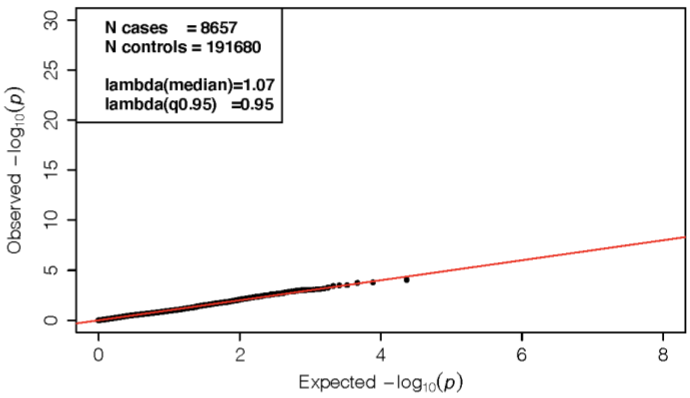
Irritable bowel syndrome
N cases = 8657
N controls = 191680
lambda(median)=1.07
lambda(q0.95) =0.95
Observed −log10(p)
Expected −log10(p)

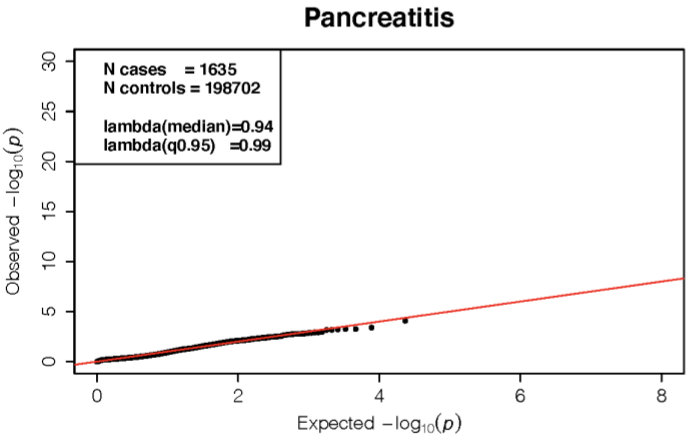
Pancreatitis
N cases = 1635
N controls = 198702
lambda(median)=0.94
lambda(q0.95) =0.99
Observed −log10(p)
Expected −log10(p)

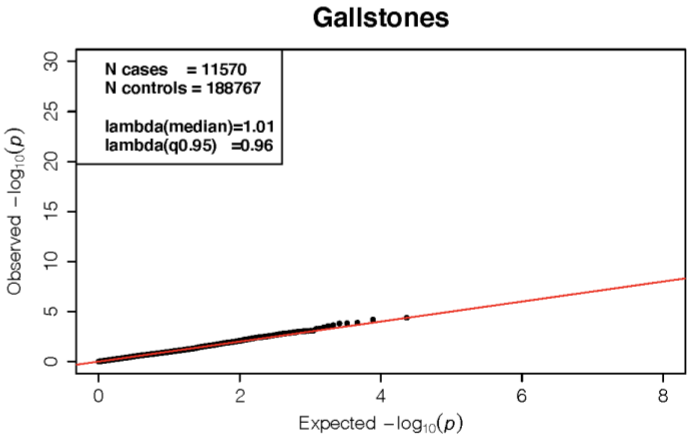
Gallstones
N cases = 11570
N controls = 188767
lambda(median)=1.01
lambda(q0.95) =0.96
Observed −log10(p)
Expected −log10(p)

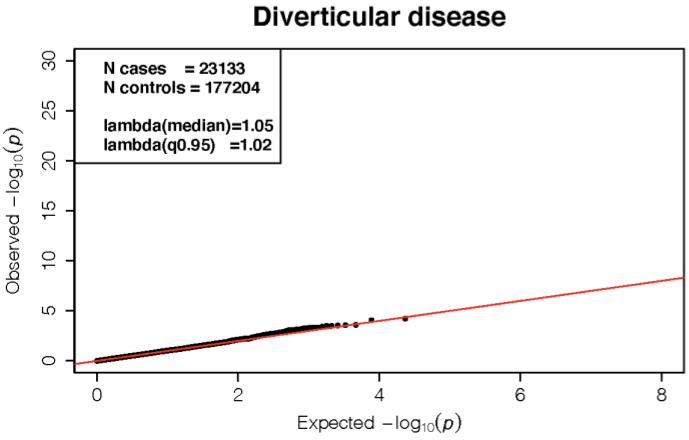
Diverticular disease
N cases = 23133
N controls = 177204
lambda(median)=1.05
lambda(q0.95) =1.02
Observed −log10(p)
Expected −log10(p)

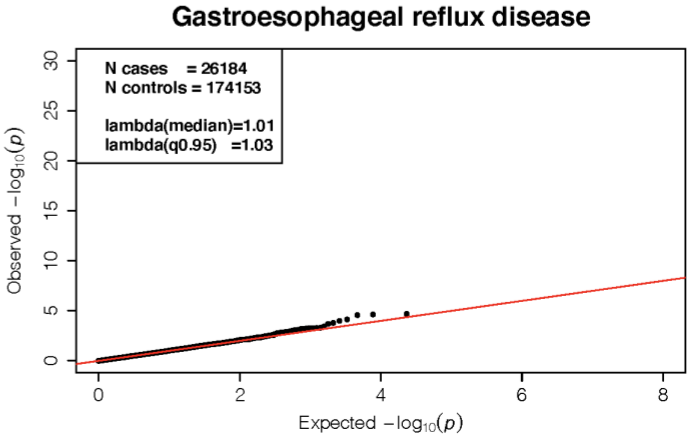
Gastroesophageal reflux disease
N cases = 26184
N controls = 174153
lambda(median)=1.01
lambda(q0.95) =1.03
Observed −log10(p)
Expected −log10(p)

461

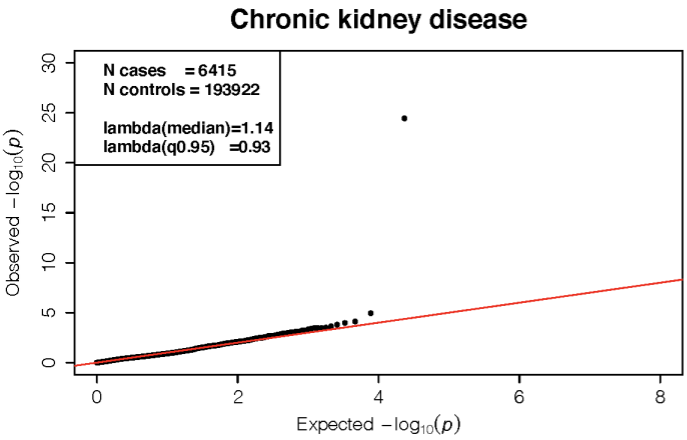
Chronic kidney disease
N cases = 6415
N controls = 193922
lambda(median)=1.14
lambda(q0.95) =0.93
Observed $-\log_{10}(p)$
Expected $-\log_{10}(p)$

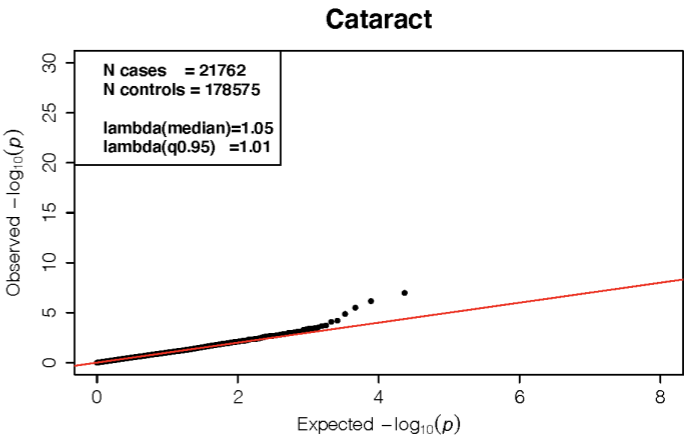
Cataract
N cases = 21762
N controls = 178575
lambda(median)=1.05
lambda(q0.95) =1.01
Observed $-\log_{10}(p)$
Expected $-\log_{10}(p)$

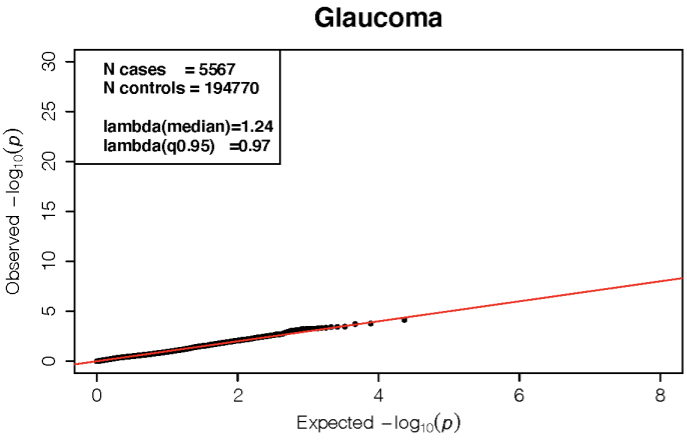
Glaucoma
N cases = 5567
N controls = 194770
lambda(median)=1.24
lambda(q0.95) =0.97
Observed $-\log_{10}(p)$
Expected $-\log_{10}(p)$

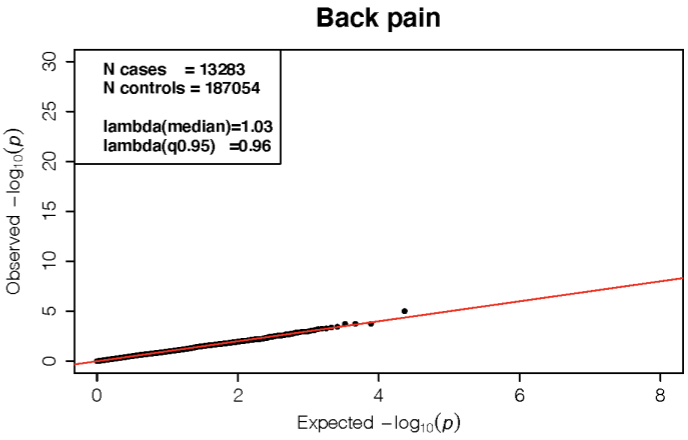
Back pain
N cases = 13283
N controls = 187054
lambda(median)=1.03
lambda(q0.95) =0.96
Observed $-\log_{10}(p)$
Expected $-\log_{10}(p)$

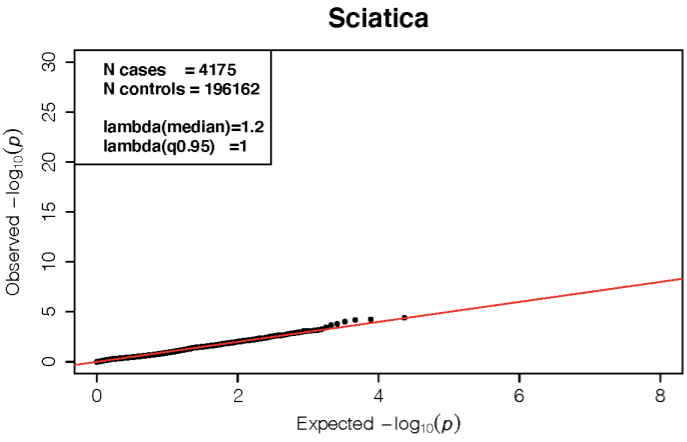
Sciatica
N cases = 4175
N controls = 196162
lambda(median)=1.2
lambda(q0.95) =1
Observed $-\log_{10}(p)$
Expected $-\log_{10}(p)$

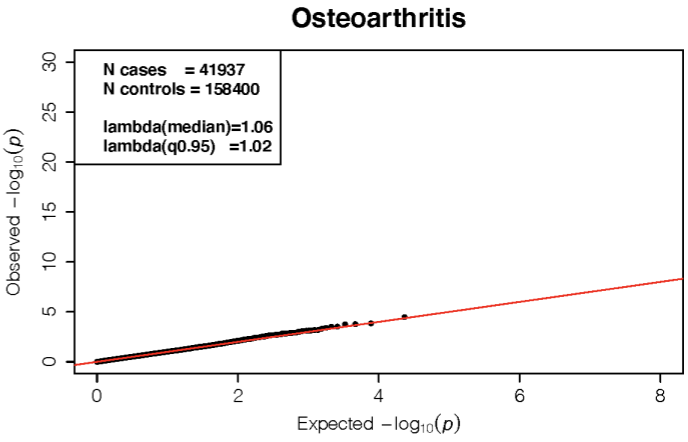
Osteoarthritis
N cases = 41937
N controls = 158400
lambda(median)=1.06
lambda(q0.95) =1.02
Observed $-\log_{10}(p)$
Expected $-\log_{10}(p)$

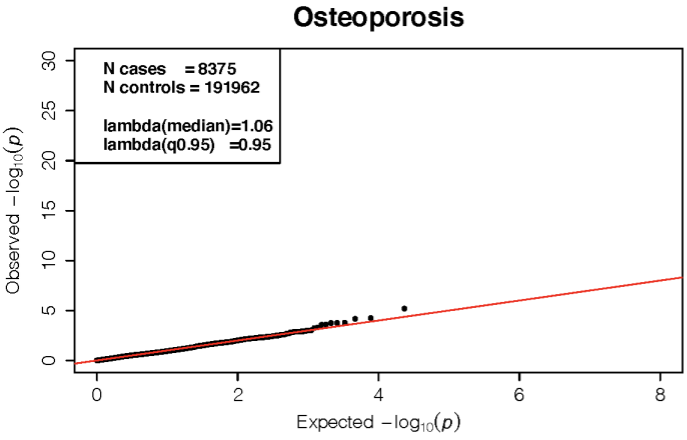
Osteoporosis
N cases = 8375
N controls = 191962
lambda(median)=1.06
lambda(q0.95) =0.95
Observed $-\log_{10}(p)$
Expected $-\log_{10}(p)$

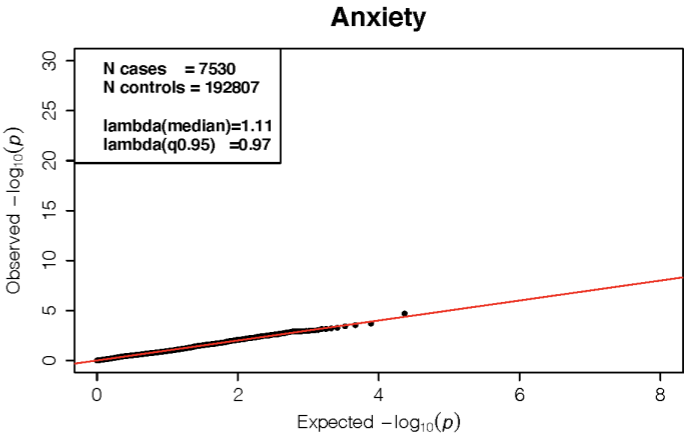
Anxiety
N cases = 7530
N controls = 192807
lambda(median)=1.11
lambda(q0.95) =0.97
Observed $-\log_{10}(p)$
Expected $-\log_{10}(p)$

462

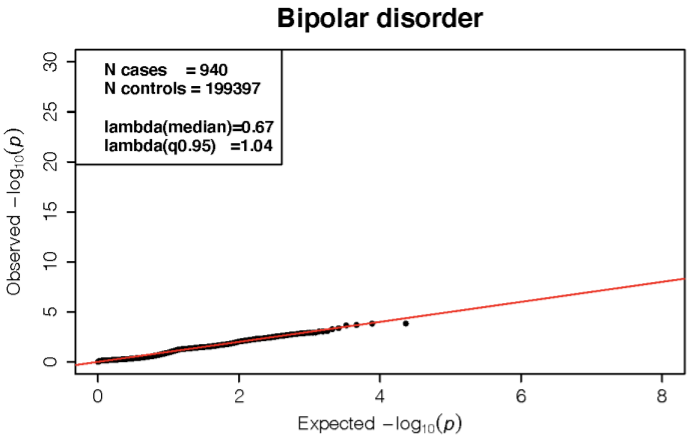
Bipolar disorder
N cases = 940
N controls = 199397
lambda(median)=0.67
lambda(q0.95) =1.04
Observed −log10(p)
Expected −log10(p)

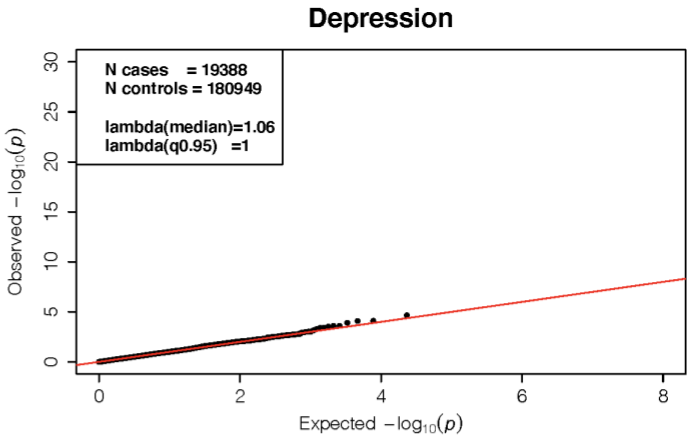
Depression
N cases = 19388
N controls = 180949
lambda(median)=1.06
lambda(q0.95) =1
Observed −log10(p)
Expected −log10(p)

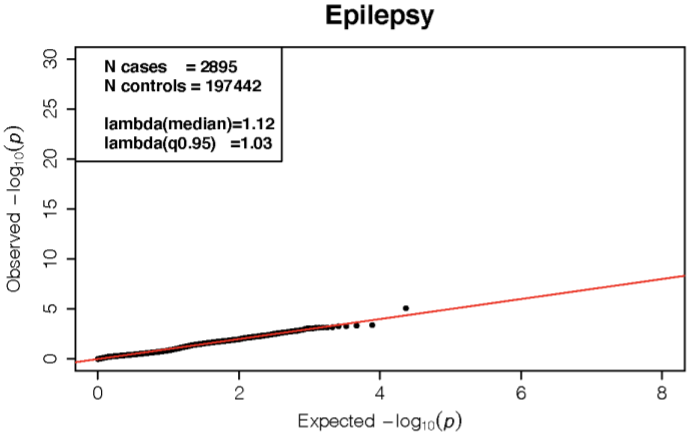
Epilepsy
N cases = 2895
N controls = 197442
lambda(median)=1.12
lambda(q0.95) =1.03
Observed −log10(p)
Expected −log10(p)

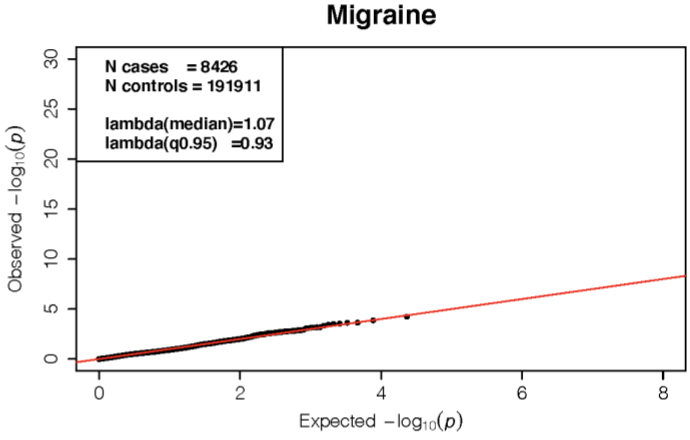
Migraine
N cases = 8426
N controls = 191911
lambda(median)=1.07
lambda(q0.95) =0.93
Observed −log10(p)
Expected −log10(p)

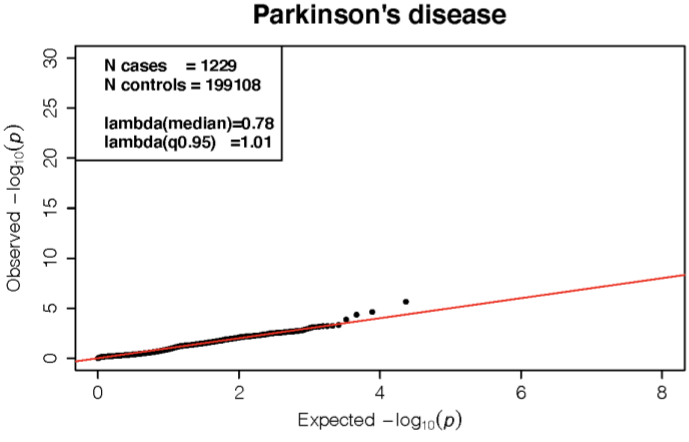
Parkinson's disease
N cases = 1229
N controls = 199108
lambda(median)=0.78
lambda(q0.95) =1.01
Observed −log10(p)
Expected −log10(p)

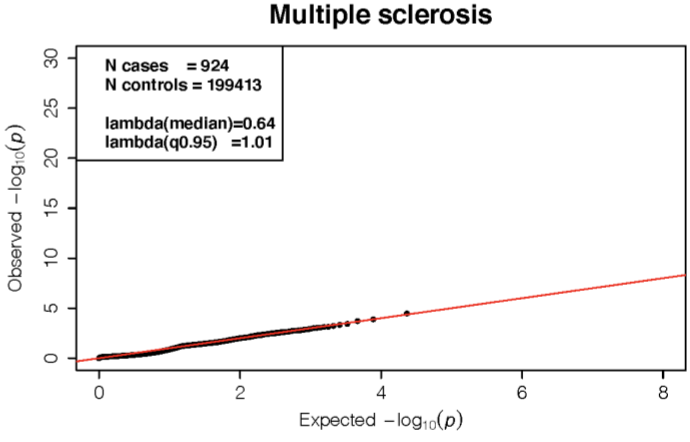
Multiple sclerosis
N cases = 924
N controls = 199413
lambda(median)=0.64
lambda(q0.95) =1.01
Observed −log10(p)
Expected −log10(p)

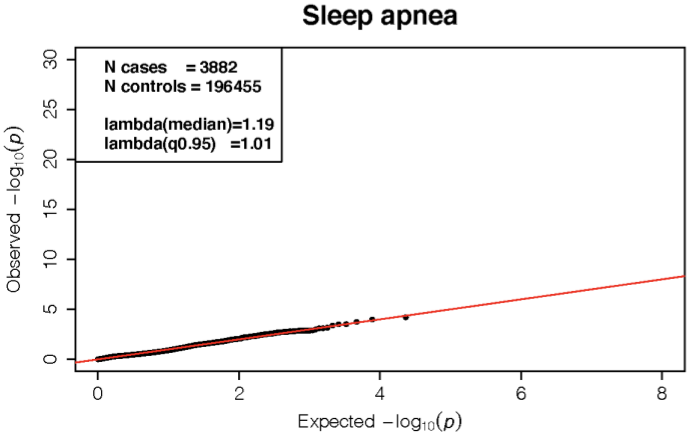
Sleep apnea
N cases = 3882
N controls = 196455
lambda(median)=1.19
lambda(q0.95) =1.01
Observed −log10(p)
Expected −log10(p)

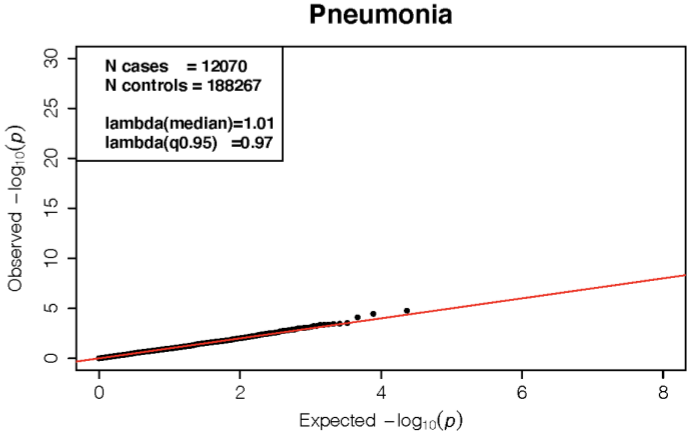
Pneumonia
N cases = 12070
N controls = 188267
lambda(median)=1.01
lambda(q0.95) =0.97
Observed −log10(p)
Expected −log10(p)

463

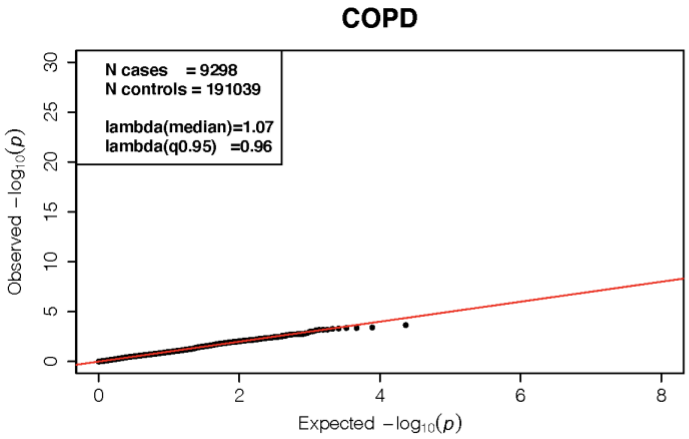


**Supplementary Figure 3: Quantile-quantile plots for exome-wide gene-based tests for each individual binary trait.** The y-axis represents the observed –log10 *P*-values across all tests, while the x-axis represents the expected under the null-hypothesis. *P*-values were obtained from saddle point approximation and were obtained from logistic mixed effects models, adjusting for sex, age, sequencing batch, associated principal components (PCs), a sparse kinship matrix. *P*-values shown are two-sided and unadjusted for multiple testing. The algorithm implemented in GENESIS applies the Saddle Point Approximation to raw *P*-values reaching $P<0.05$ to account for case-control imbalance. As such, *P*-values larger than 0.05 might not be well calibrated and λ estimated at the median of the *P*-value distribution might not capture the calibration of the tests. We therefore estimated the λ values for binary traits at the tail of the distributions, λ(q0.95), by comparing the test statistic at the 95$^{th}$ quantile to the expected statistic at this quantile under the null. Visually, and by judging λ(q0.95), none of the binary traits showed major systemic inflation.

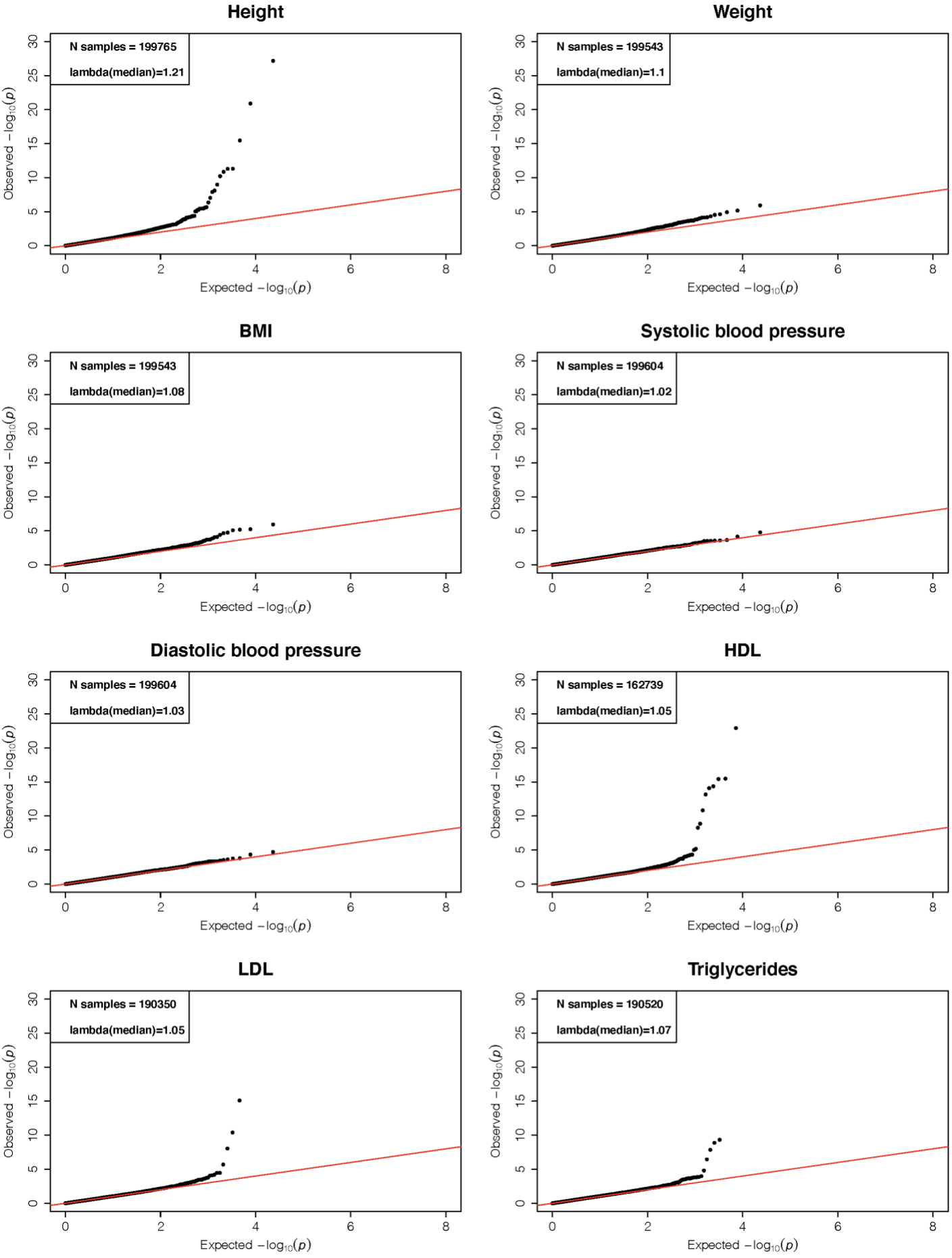
Height
N samples = 199765
lambda(median)=1.21
Weight
N samples = 199543
lambda(median)=1.1
BMI
N samples = 199543
lambda(median)=1.08
Systolic blood pressure
N samples = 199604
lambda(median)=1.02
Diastolic blood pressure
N samples = 199604
lambda(median)=1.03
HDL
N samples = 162739
lambda(median)=1.05
LDL
N samples = 190350
lambda(median)=1.05
Triglycerides
N samples = 190520
lambda(median)=1.07
Observed $-\log_{10}(p)$
Expected $-\log_{10}(p)$

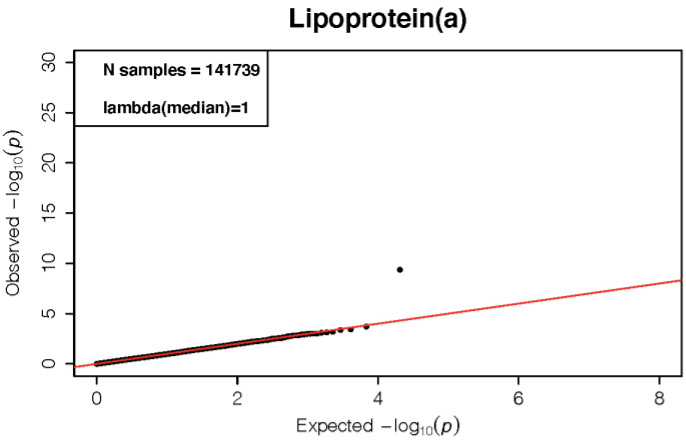
Lipoprotein(a)
N samples = 141739
lambda(median)=1
Observed $-\log_{10}(p)$
Expected $-\log_{10}(p)$

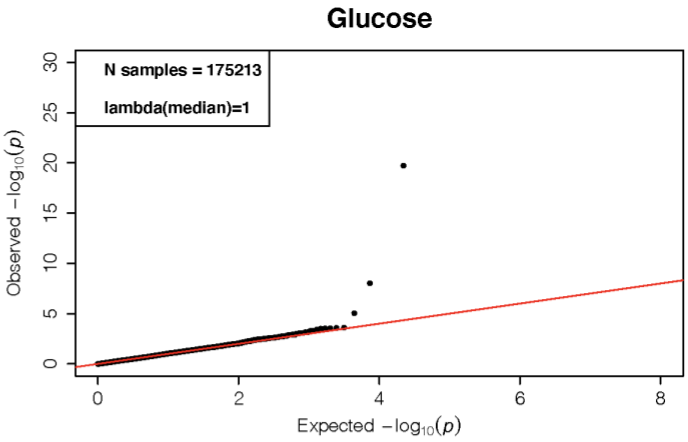
Glucose
N samples = 175213
lambda(median)=1
Observed $-\log_{10}(p)$
Expected $-\log_{10}(p)$

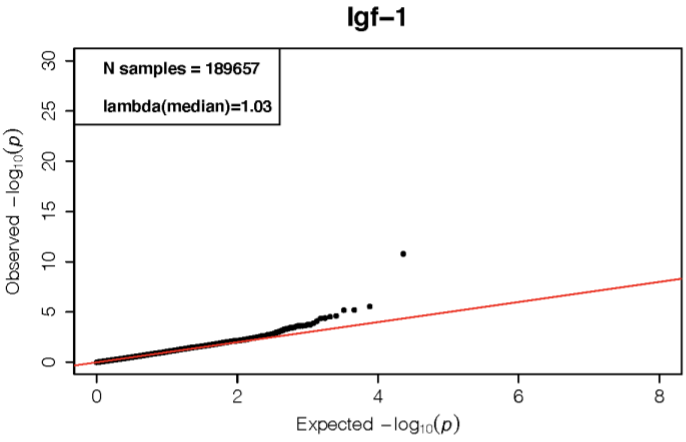
Igf−1
N samples = 189657
lambda(median)=1.03
Observed $-\log_{10}(p)$
Expected $-\log_{10}(p)$

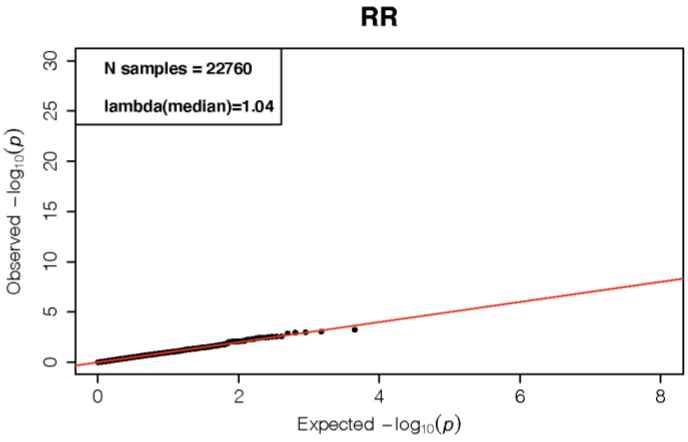
RR
N samples = 22760
lambda(median)=1.04
Observed $-\log_{10}(p)$
Expected $-\log_{10}(p)$

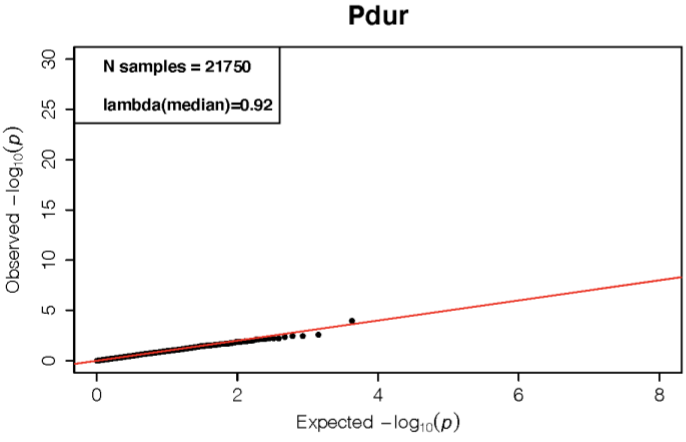
Pdur
N samples = 21750
lambda(median)=0.92
Observed $-\log_{10}(p)$
Expected $-\log_{10}(p)$

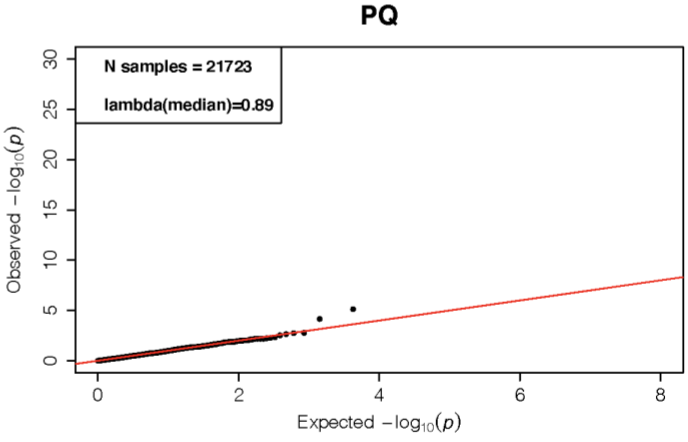
PQ
N samples = 21723
lambda(median)=0.89
Observed $-\log_{10}(p)$
Expected $-\log_{10}(p)$

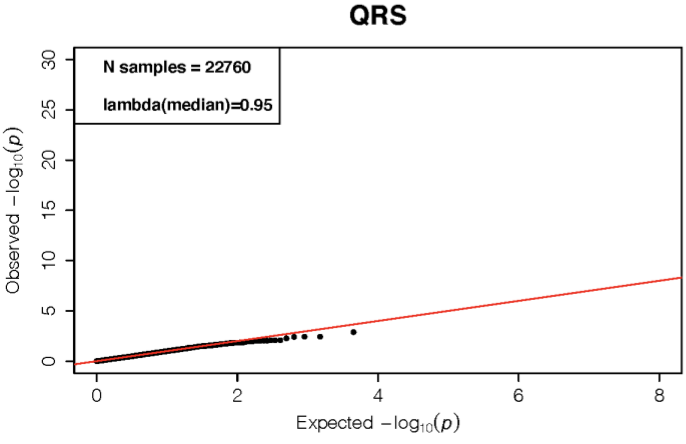
QRS
N samples = 22760
lambda(median)=0.95
Observed $-\log_{10}(p)$
Expected $-\log_{10}(p)$

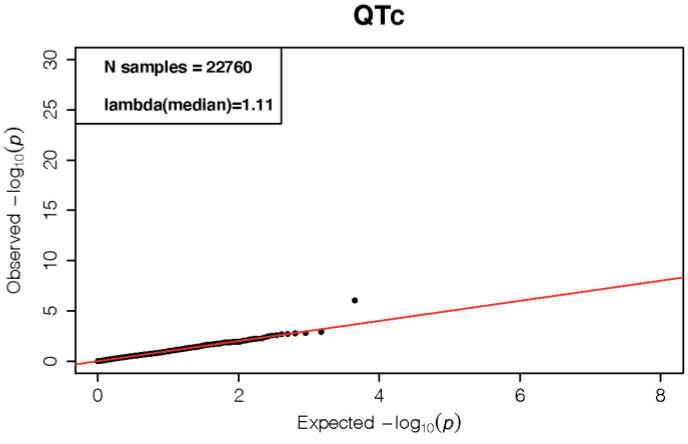
QTc
N samples = 22760
lambda(median)=1.11
Observed $-\log_{10}(p)$
Expected $-\log_{10}(p)$

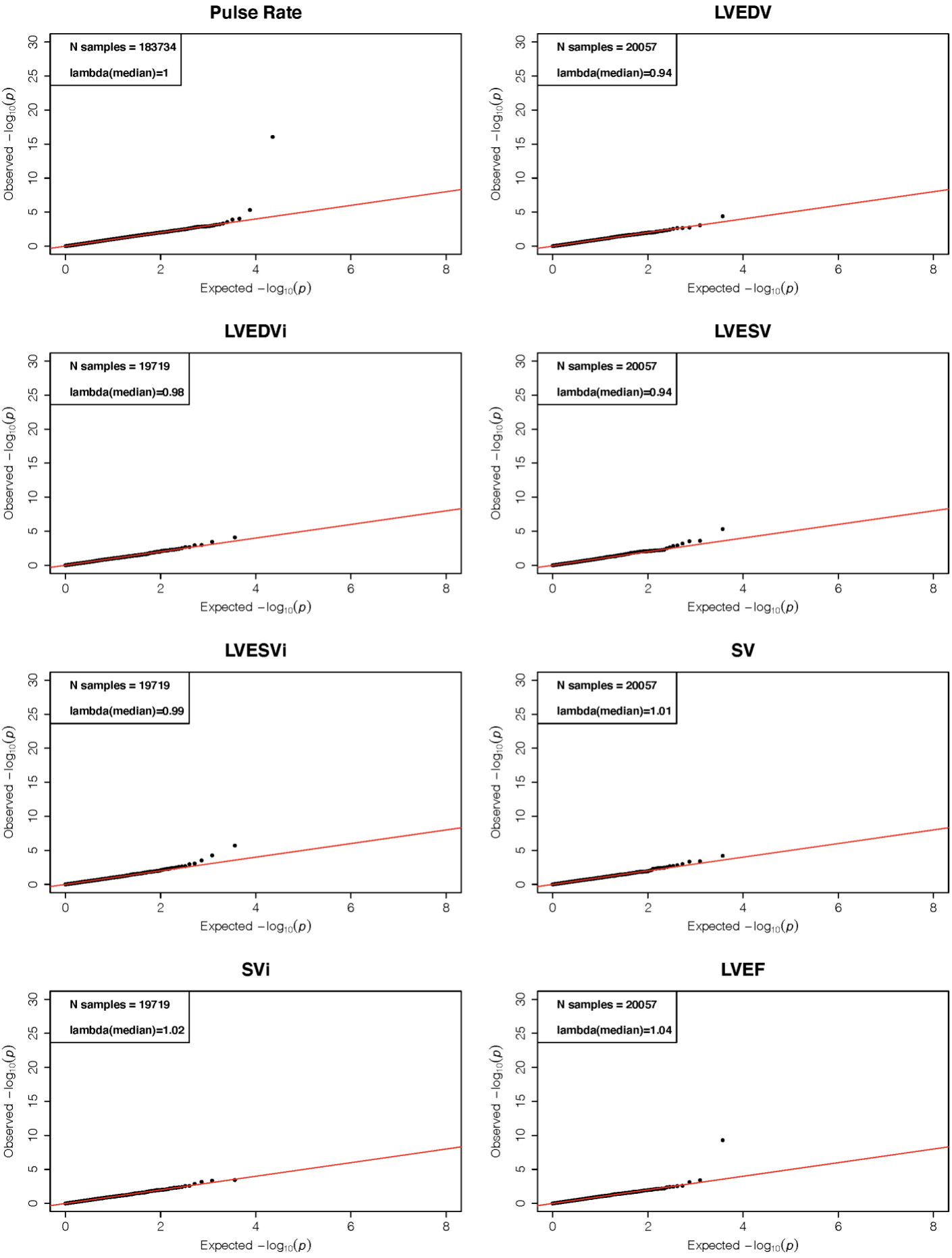
Pulse Rate
N samples = 183734
lambda(median)=1
LVEDV
N samples = 20057
lambda(median)=0.94
LVEDVi
N samples = 19719
lambda(median)=0.98
LVESV
N samples = 20057
lambda(median)=0.94
LVESVi
N samples = 19719
lambda(median)=0.99
SV
N samples = 20057
lambda(median)=1.01
SVi
N samples = 19719
lambda(median)=1.02
LVEF
N samples = 20057
lambda(median)=1.04
Observed $-\log_{10}(p)$
Expected $-\log_{10}(p)$

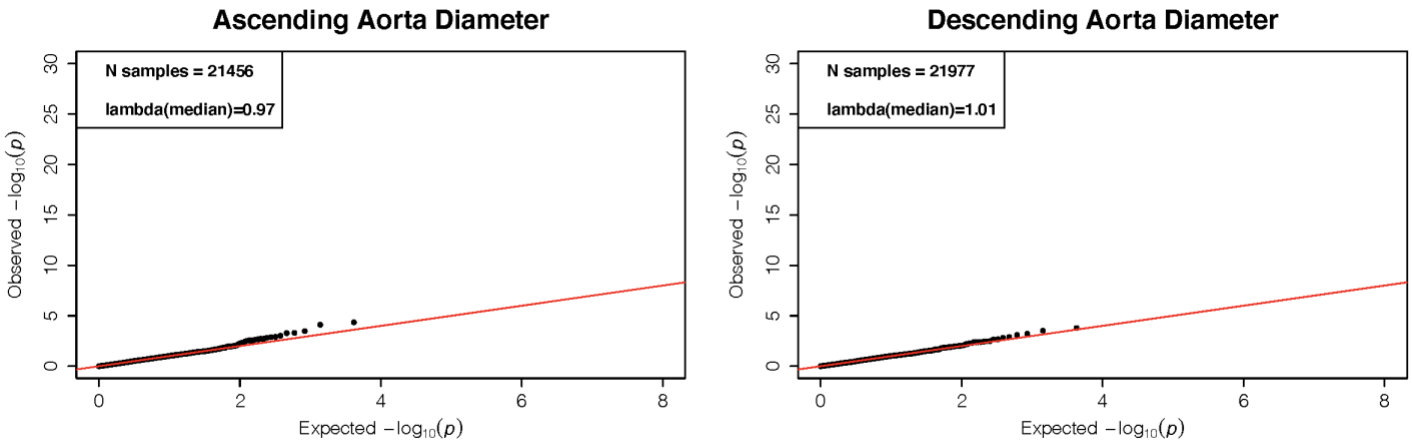


**Supplementary Figure 4: Quantile-quantile plots for exome-wide gene-based tests for each individual quantitative trait.** The y-axis represents the observed –log10 *P*-values across all tests, while the x-axis represents the expected under the null-hypothesis. *P*-values were obtained from score tests in linear mixed effects models, adjusting for sex, age, sequencing batch, associated principal components (PCs), MRI serial number (for MRI traits) and a sparse kinship matrix. *P*-values shown are two-sided and unadjusted for multiple testing. Values of λ were estimated at the median of the test statistic distribution. For three traits, height, weight and QTc, λ(median) was larger than 1.1. Height and weight indeed show a visual inflation.

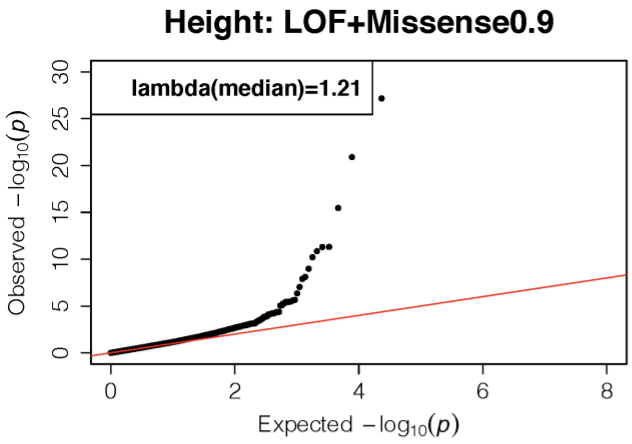
Height: LOF+Missense0.9
lambda(median)=1.21
Observed $-\log_{10}(p)$
Expected $-\log_{10}(p)$

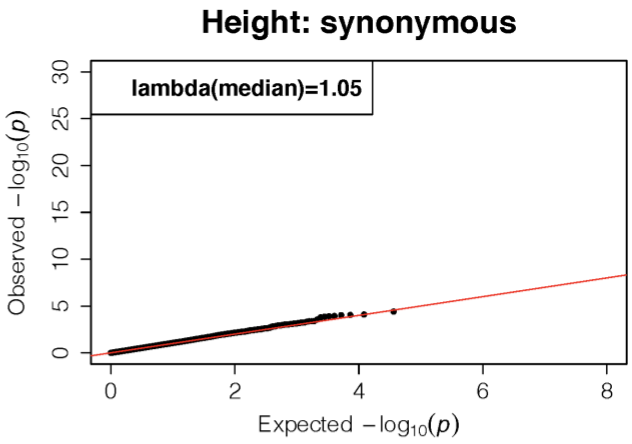
Height: synonymous
lambda(median)=1.05
Observed $-\log_{10}(p)$
Expected $-\log_{10}(p)$

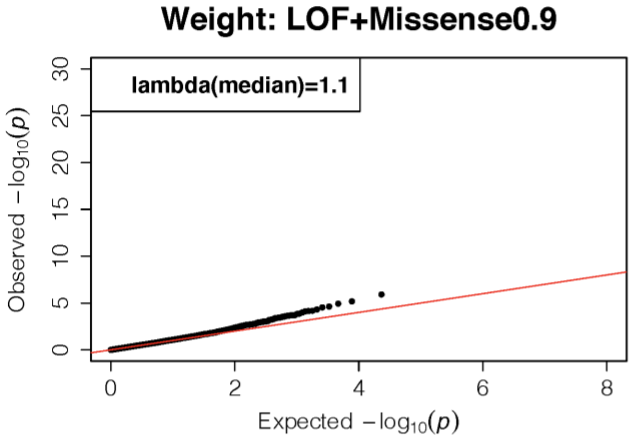
Weight: LOF+Missense0.9
lambda(median)=1.1
Observed $-\log_{10}(p)$
Expected $-\log_{10}(p)$

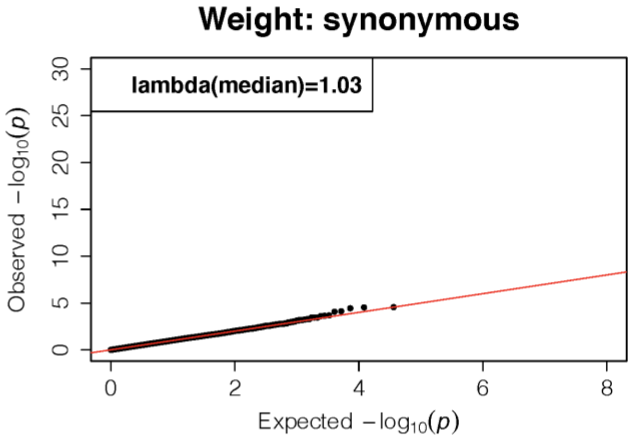
Weight: synonymous
lambda(median)=1.03
Observed $-\log_{10}(p)$
Expected $-\log_{10}(p)$

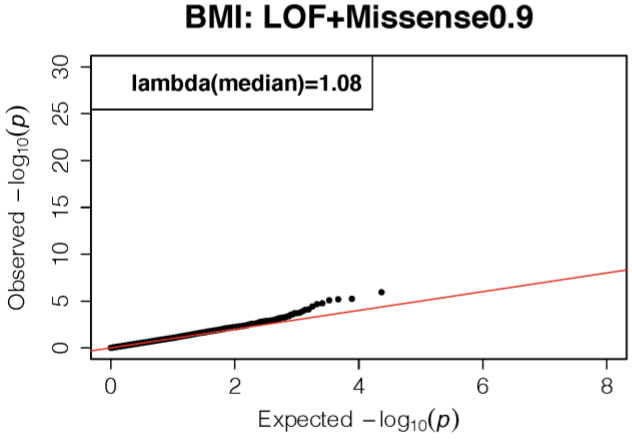
BMI: LOF+Missense0.9
lambda(median)=1.08
Observed $-\log_{10}(p)$
Expected $-\log_{10}(p)$

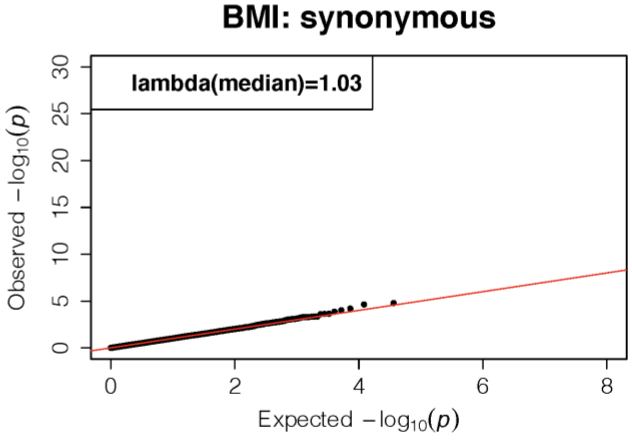
BMI: synonymous
lambda(median)=1.03
Observed $-\log_{10}(p)$
Expected $-\log_{10}(p)$

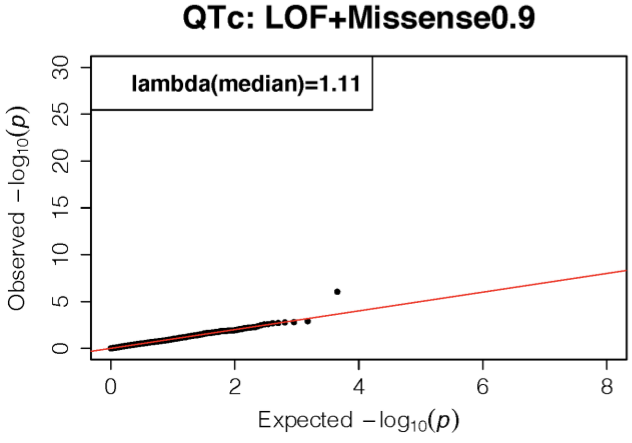
QTc: LOF+Missense0.9
lambda(median)=1.11
Observed $-\log_{10}(p)$
Expected $-\log_{10}(p)$

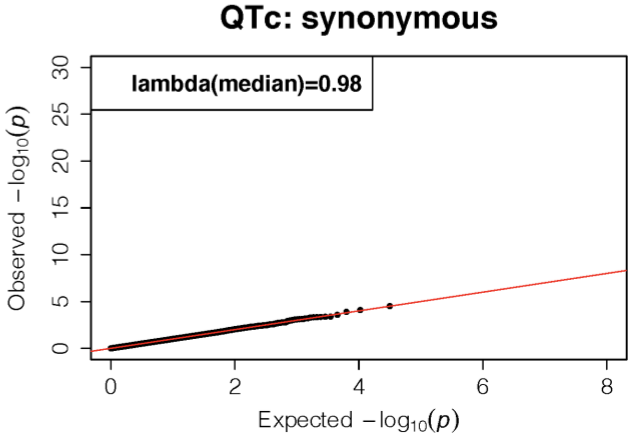
QTc: synonymous
lambda(median)=0.98
Observed $-\log_{10}(p)$
Expected $-\log_{10}(p)$

487

**Supplementary Figure 5: Quantile-quantile plots for rare deleterious variants compared to rare synonymous variants for height, weight, BMI, and QTc.** The y-axis represents the observed –log10 *P*-values across all tests, while the x-axis represents the expected under the null-hypothesis. *P*-values were obtained from score tests in linear mixed effects models, adjusting for sex, age, sequencing batch, associated principal components (PCs), MRI serial number (for MRI traits) and a sparse kinship matrix. *P*-values shown are two-sided and unadjusted for multiple testing. Left panels represent the exome-wide discovery analysis where we analyzed rare LOF and predicted deleterious missense variants, while the right panels show the results for rare (MAF<0.1%) synonymous variants. As expected under the null, the distributions for the synonymous variants do not show inflation.

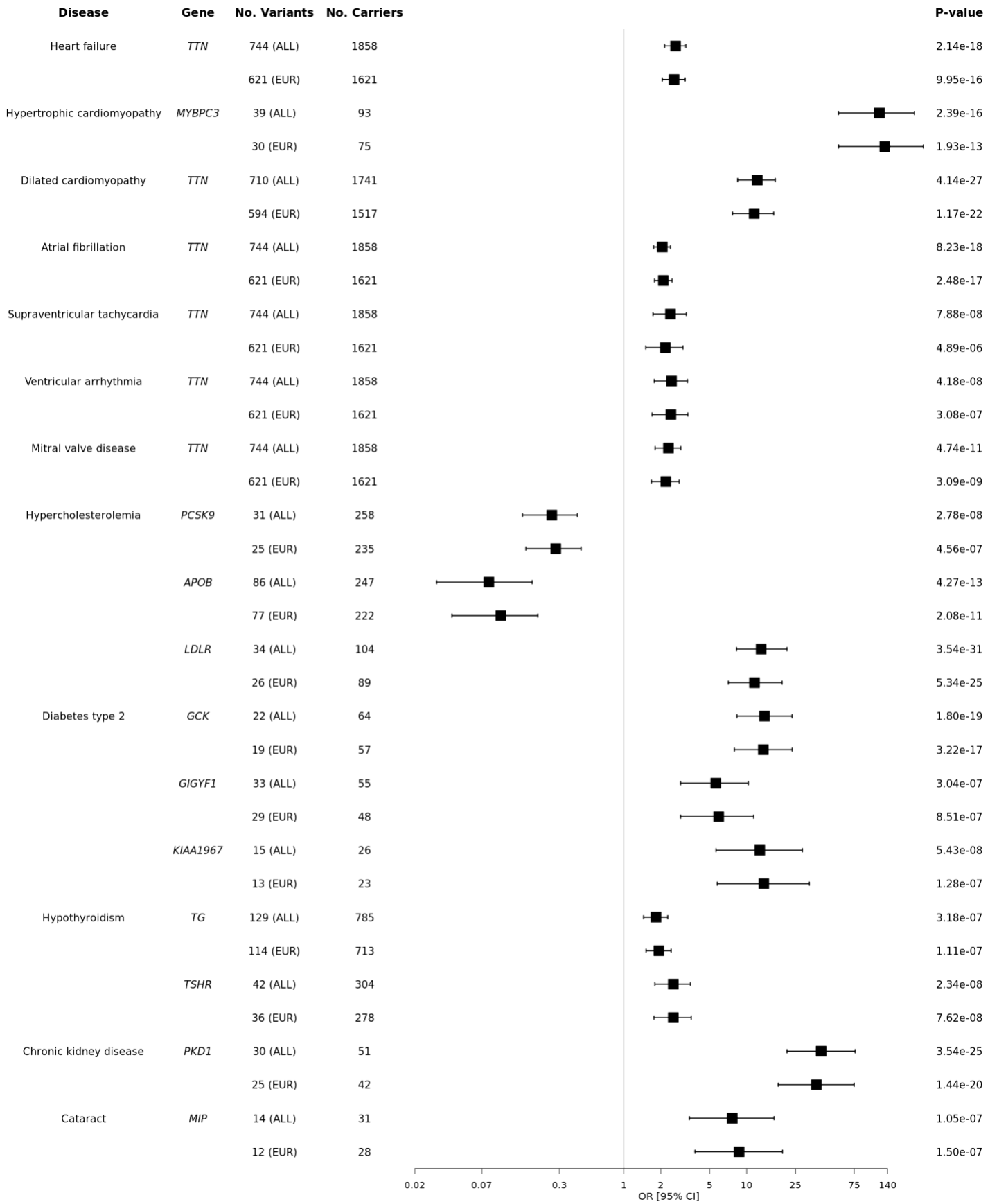
Disease
Gene
No. Variants
No. Carriers
P-value
Heart failure
TTN
744 (ALL)
1858
2.14e-18
621 (EUR)
1621
9.95e-16
Hypertrophic cardiomyopathy
MYBPC3
39 (ALL)
93
2.39e-16
30 (EUR)
75
1.93e-13
Dilated cardiomyopathy
TTN
710 (ALL)
1741
4.14e-27
594 (EUR)
1517
1.17e-22
Atrial fibrillation
TTN
744 (ALL)
1858
8.23e-18
621 (EUR)
1621
2.48e-17
Supraventricular tachycardia
TTN
744 (ALL)
1858
7.88e-08
621 (EUR)
1621
4.89e-06
Ventricular arrhythmia
TTN
744 (ALL)
1858
4.18e-08
621 (EUR)
1621
3.08e-07
Mitral valve disease
TTN
744 (ALL)
1858
4.74e-11
621 (EUR)
1621
3.09e-09
Hypercholesterolemia
PCSK9
31 (ALL)
258
2.78e-08
25 (EUR)
235
4.56e-07
APOB
86 (ALL)
247
4.27e-13
77 (EUR)
222
2.08e-11
LDLR
34 (ALL)
104
3.54e-31
26 (EUR)
89
5.34e-25
Diabetes type 2
GCK
22 (ALL)
64
1.80e-19
19 (EUR)
57
3.22e-17
GIGYF1
33 (ALL)
55
3.04e-07
29 (EUR)
48
8.51e-07
KIAA1967
15 (ALL)
26
5.43e-08
13 (EUR)
23
1.28e-07
Hypothyroidism
TG
129 (ALL)
785
3.18e-07
114 (EUR)
713
1.11e-07
TSHR
42 (ALL)
304
2.34e-08
36 (EUR)
278
7.62e-08
Chronic kidney disease
PKD1
30 (ALL)
51
3.54e-25
25 (EUR)
42
1.44e-20
Cataract
MIP
14 (ALL)
31
1.05e-07
12 (EUR)
28
1.50e-07
0.02
0.07
0.3
1
2
5
10
25
75
140
OR [95% CI]

**Supplementary Figure 6. Sensitivity analysis restricting to individuals of European ancestry only in the analysis of binary traits.** Data are presented as Odds Ratios (OR) with error bars representing 95% confidence intervals (CI). *P*-values were computed using saddle point approximation and were obtained from logistic mixed effects models, adjusting for sex, age, sequencing batch, associated principal components (PCs), a sparse kinship matrix. *P*-values shown are two-sided and unadjusted for multiple testing. ORs and CIs were obtained from Firth's regression models adjusting for sex, age, sequencing batch and associated PCs among unrelated samples. *P*-values are two-sided and unadjusted for multiple testing. Exome-wide significant associations for binary traits were largely consistent when restricting to a homogenous subset of the cohort consisting of European individuals only. Abbreviations: ALL, all ancestry individuals included; EUR, European ancestry individuals only.

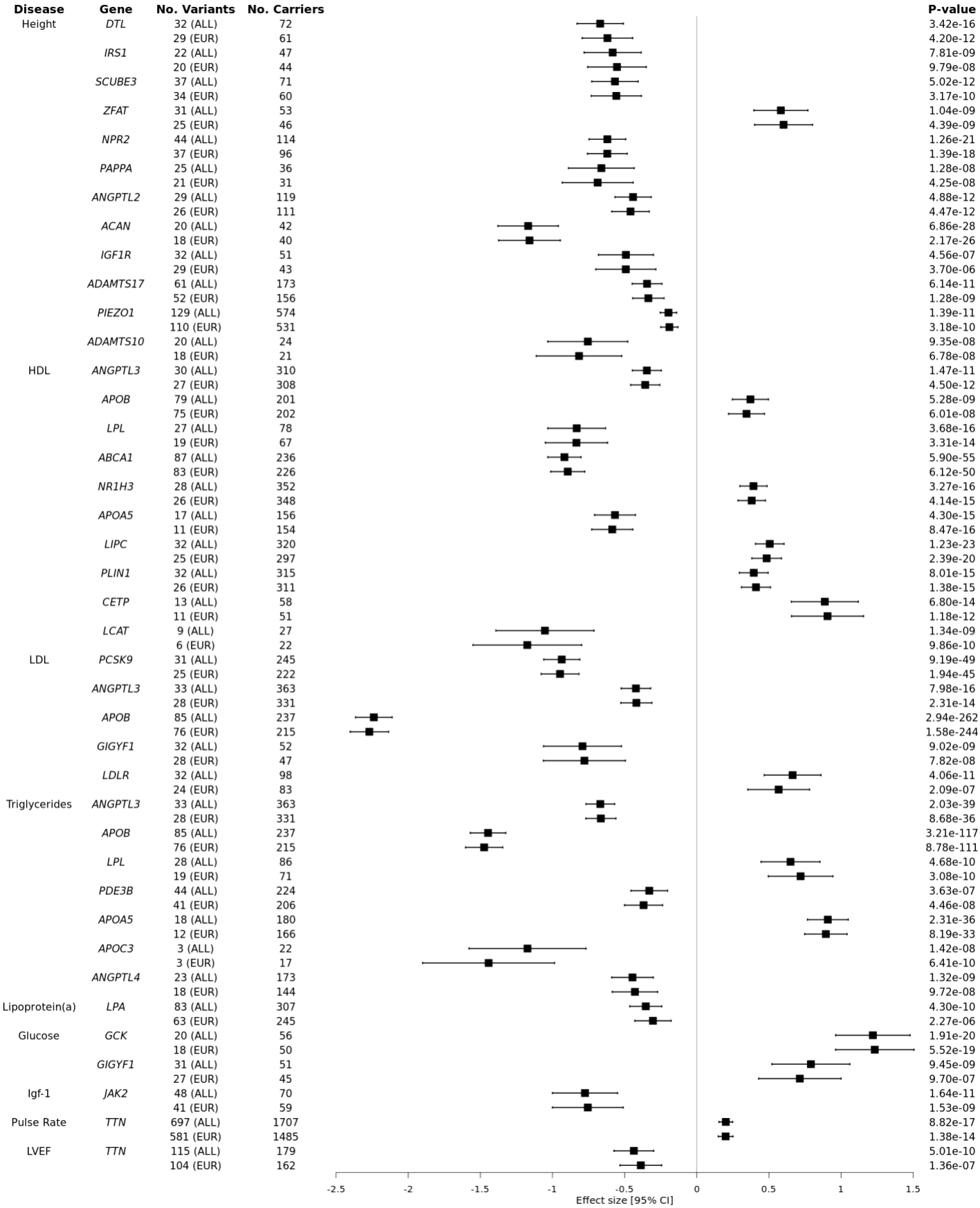
Disease
Gene
No. Variants
No. Carriers
P-value
Height DTL 32 (ALL) 72 3.42e-16
29 (EUR) 61 4.20e-12
IRS1 22 (ALL) 47 7.81e-09
20 (EUR) 44 9.79e-08
SCUBE3 37 (ALL) 71 5.02e-12
34 (EUR) 60 3.17e-10
ZFAT 31 (ALL) 53 1.04e-09
25 (EUR) 46 4.39e-09
NPR2 44 (ALL) 114 1.26e-21
37 (EUR) 96 1.39e-18
PAPPA 25 (ALL) 36 1.28e-08
21 (EUR) 31 4.25e-08
ANGPTL2 29 (ALL) 119 4.88e-12
26 (EUR) 111 4.47e-12
ACAN 20 (ALL) 42 6.86e-28
18 (EUR) 40 2.17e-26
IGF1R 32 (ALL) 51 4.56e-07
29 (EUR) 43 3.70e-06
ADAMTS17 61 (ALL) 173 6.14e-11
52 (EUR) 156 1.28e-09
PIEZO1 129 (ALL) 574 1.39e-11
110 (EUR) 531 3.18e-10
ADAMTS10 20 (ALL) 24 9.35e-08
18 (EUR) 21 6.78e-08
HDL ANGPTL3 30 (ALL) 310 1.47e-11
27 (EUR) 308 4.50e-12
APOB 79 (ALL) 201 5.28e-09
75 (EUR) 202 6.01e-08
LPL 27 (ALL) 78 3.68e-16
19 (EUR) 67 3.31e-14
ABCA1 87 (ALL) 236 5.90e-55
83 (EUR) 226 6.12e-50
NR1H3 28 (ALL) 352 3.27e-16
26 (EUR) 348 4.14e-15
APOA5 17 (ALL) 156 4.30e-15
11 (EUR) 154 8.47e-16
LIPC 32 (ALL) 320 1.23e-23
25 (EUR) 297 2.39e-20
PLIN1 32 (ALL) 315 8.01e-15
26 (EUR) 311 1.38e-15
CETP 13 (ALL) 58 6.80e-14
11 (EUR) 51 1.18e-12
LCAT 9 (ALL) 27 1.34e-09
6 (EUR) 22 9.86e-10
LDL PCSK9 31 (ALL) 245 9.19e-49
25 (EUR) 222 1.94e-45
ANGPTL3 33 (ALL) 363 7.98e-16
28 (EUR) 331 2.31e-14
APOB 85 (ALL) 237 2.94e-262
76 (EUR) 215 1.58e-244
GIGYF1 32 (ALL) 52 9.02e-09
28 (EUR) 47 7.82e-08
LDLR 32 (ALL) 98 4.06e-11
24 (EUR) 83 2.09e-07
Triglycerides ANGPTL3 33 (ALL) 363 2.03e-39
28 (EUR) 331 8.68e-36
APOB 85 (ALL) 237 3.21e-117
76 (EUR) 215 8.78e-111
LPL 28 (ALL) 86 4.68e-10
19 (EUR) 71 3.08e-10
PDE3B 44 (ALL) 224 3.63e-07
41 (EUR) 206 4.46e-08
APOA5 18 (ALL) 180 2.31e-36
12 (EUR) 166 8.19e-33
APOC3 3 (ALL) 22 1.42e-08
3 (EUR) 17 6.41e-10
ANGPTL4 23 (ALL) 173 1.32e-09
18 (EUR) 144 9.72e-08
Lipoprotein(a) LPA 83 (ALL) 307 4.30e-10
63 (EUR) 245 2.27e-06
Glucose GCK 20 (ALL) 56 1.91e-20
18 (EUR) 50 5.52e-19
GIGYF1 31 (ALL) 51 9.45e-09
27 (EUR) 45 9.70e-07
Igf-1 JAK2 48 (ALL) 70 1.64e-11
41 (EUR) 59 1.53e-09
Pulse Rate TTN 697 (ALL) 1707 8.82e-17
581 (EUR) 1485 1.38e-14
LVEF TTN 115 (ALL) 179 5.01e-10
104 (EUR) 162 1.36e-07
-2.5
-2
-1.5
-1
-0.5
0
0.5
1
1.5
Effect size [95% CI]

**Supplementary Figure 7. Sensitivity analysis restricting to individuals of European ancestry only in the analysis of quantitative traits.** Data are presented as effect size (β) estimates per standard deviation with error bars representing 95% confidence intervals (CI). *P*-values, effect sizes and 95% CIs were obtained from score tests in linear mixed effects models, adjusting for sex, age, sequencing batch, associated principal components (PCs), MRI serial number (for MRI traits) and a sparse kinship matrix. *P*-values shown are unadjusted for multiple testing. Associations were largely consistent when restricting to samples from a homogenous subset of European individuals only. Abbreviations: ALL, all ancestry individuals included; EUR, European ancestry individuals only; CI, confidence interval; HDL, high-density lipoprotein; LDL, low-density lipoprotein; Igf-1, insulin-like growth factor-1; QTc, Bazett-corrected QT interval; LVEF, left ventricular ejection fraction; CI, confidence interval.

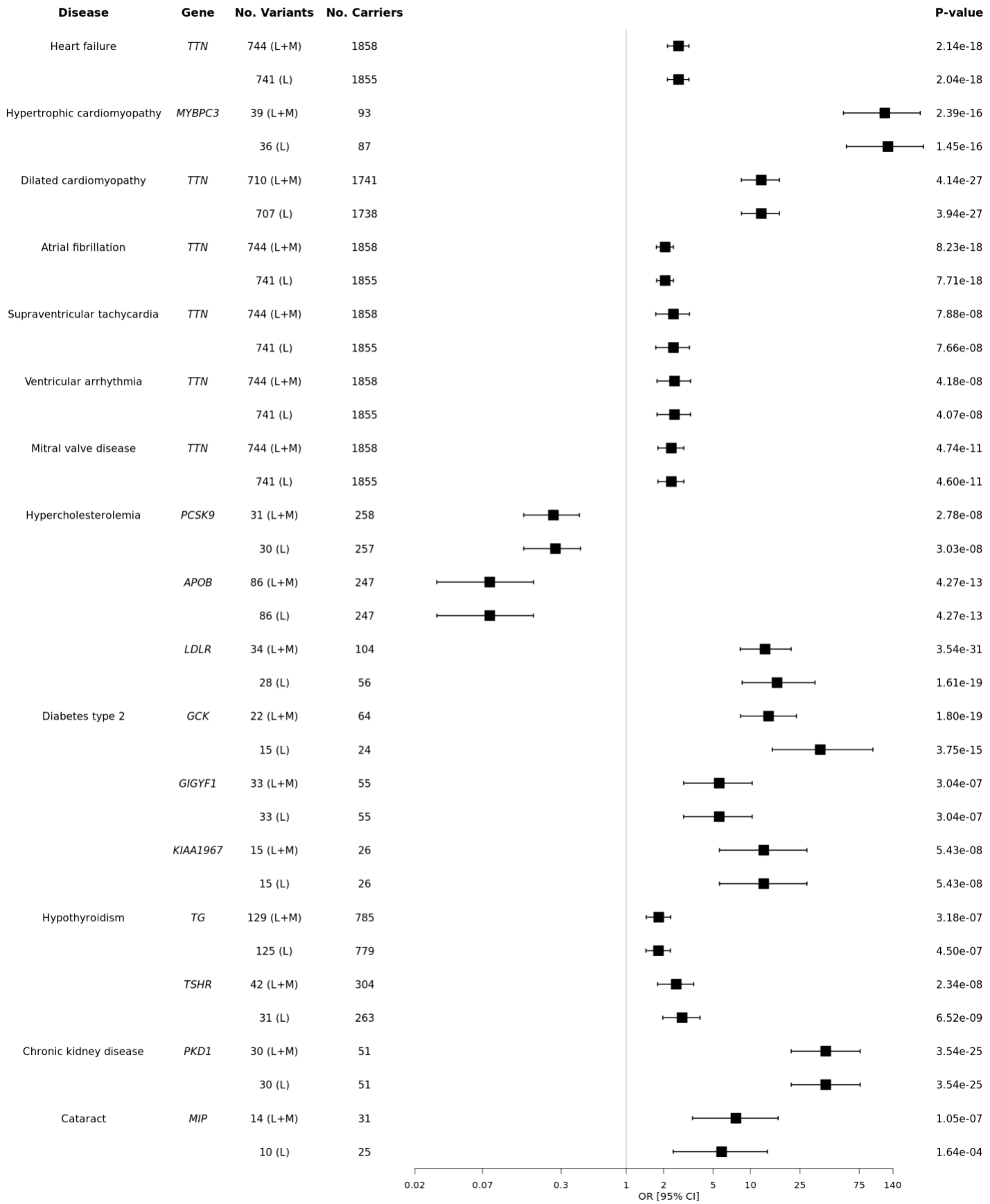
Disease
Gene
No. Variants
No. Carriers
P-value
Heart failure
TTN
744 (L+M)
1858
2.14e-18
741 (L)
1855
2.04e-18
Hypertrophic cardiomyopathy
MYBPC3
39 (L+M)
93
2.39e-16
36 (L)
87
1.45e-16
Dilated cardiomyopathy
TTN
710 (L+M)
1741
4.14e-27
707 (L)
1738
3.94e-27
Atrial fibrillation
TTN
744 (L+M)
1858
8.23e-18
741 (L)
1855
7.71e-18
Supraventricular tachycardia
TTN
744 (L+M)
1858
7.88e-08
741 (L)
1855
7.66e-08
Ventricular arrhythmia
TTN
744 (L+M)
1858
4.18e-08
741 (L)
1855
4.07e-08
Mitral valve disease
TTN
744 (L+M)
1858
4.74e-11
741 (L)
1855
4.60e-11
Hypercholesterolemia
PCSK9
31 (L+M)
258
2.78e-08
30 (L)
257
3.03e-08
APOB
86 (L+M)
247
4.27e-13
86 (L)
247
4.27e-13
LDLR
34 (L+M)
104
3.54e-31
28 (L)
56
1.61e-19
Diabetes type 2
GCK
22 (L+M)
64
1.80e-19
15 (L)
24
3.75e-15
GIGYF1
33 (L+M)
55
3.04e-07
33 (L)
55
3.04e-07
KIAA1967
15 (L+M)
26
5.43e-08
15 (L)
26
5.43e-08
Hypothyroidism
TG
129 (L+M)
785
3.18e-07
125 (L)
779
4.50e-07
TSHR
42 (L+M)
304
2.34e-08
31 (L)
263
6.52e-09
Chronic kidney disease
PKD1
30 (L+M)
51
3.54e-25
30 (L)
51
3.54e-25
Cataract
MIP
14 (L+M)
31
1.05e-07
10 (L)
25
1.64e-04
0.02
0.07
0.3
1
2
5
10
25
75
140
OR [95% CI]

**Supplementary Figure 8. Sensitivity analysis restricting to LOFs only in the primary analysis of binary traits.** Data are presented as Odds Ratios (OR) with error bars representing 95% confidence intervals (CI). *P*-values were computed using the saddle point approximation and were obtained from logistic mixed effects models, adjusting for sex, age, sequencing batch, associated principal components (PCs), a sparse kinship matrix. *P*-values shown are two-sided and unadjusted for multiple testing. ORs and CIs were obtained from Firth's regression models adjusting for sex, age, sequencing batch and associated PCs among unrelated samples. *P*-values are two-sided and unadjusted for multiple testing. Effect estimates for analysis of LOFs were largely consistent with effect estimates from LOFs and predicted-damaging missense combined, indicating that in general effect sizes from our discovery analysis our not diluted by the included missense variants. However, effect sizes were attenuated by including missense variants for *GCK*/type 2 diabetes. Interestingly, the *GCK*/diabetes association also dropped in significance after removing missense variants; this indicates that a number of these missense variants were functional, possibly with smaller effect sizes than LOFs. Abbreviations: L, high-confidence loss-of-function variants only; L+M, high-confidence loss-of-function and predicted-damaging missense variants combined; CI, confidence interval.

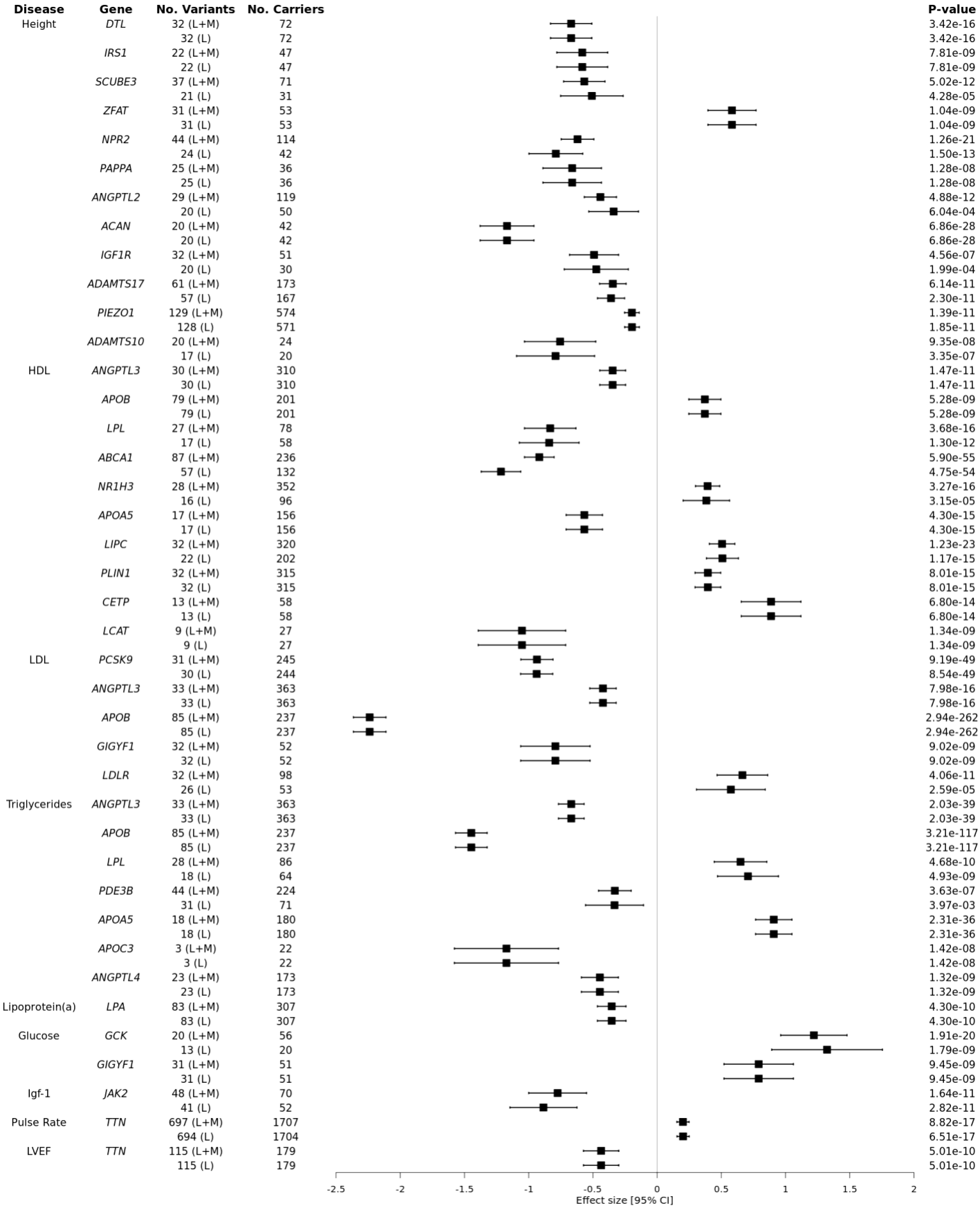
Disease
Gene
No. Variants
No. Carriers
P-value
Height DTL 32 (L+M) 72 3.42e-16
32 (L) 72 3.42e-16
IRS1 22 (L+M) 47 7.81e-09
22 (L) 47 7.81e-09
SCUBE3 37 (L+M) 71 5.02e-12
21 (L) 31 4.28e-05
ZFAT 31 (L+M) 53 1.04e-09
31 (L) 53 1.04e-09
NPR2 44 (L+M) 114 1.26e-21
24 (L) 42 1.50e-13
PAPPA 25 (L+M) 36 1.28e-08
25 (L) 36 1.28e-08
ANGPTL2 29 (L+M) 119 4.88e-12
20 (L) 50 6.04e-04
ACAN 20 (L+M) 42 6.86e-28
20 (L) 42 6.86e-28
IGF1R 32 (L+M) 51 4.56e-07
20 (L) 30 1.99e-04
ADAMTS17 61 (L+M) 173 6.14e-11
57 (L) 167 2.30e-11
PIEZO1 129 (L+M) 574 1.39e-11
128 (L) 571 1.85e-11
ADAMTS10 20 (L+M) 24 9.35e-08
17 (L) 20 3.35e-07
HDL ANGPTL3 30 (L+M) 310 1.47e-11
30 (L) 310 1.47e-11
APOB 79 (L+M) 201 5.28e-09
79 (L) 201 5.28e-09
LPL 27 (L+M) 78 3.68e-16
17 (L) 58 1.30e-12
ABCA1 87 (L+M) 236 5.90e-55
57 (L) 132 4.75e-54
NR1H3 28 (L+M) 352 3.27e-16
16 (L) 96 3.15e-05
APOA5 17 (L+M) 156 4.30e-15
17 (L) 156 4.30e-15
LIPC 32 (L+M) 320 1.23e-23
22 (L) 202 1.17e-15
PLIN1 32 (L+M) 315 8.01e-15
32 (L) 315 8.01e-15
CETP 13 (L+M) 58 6.80e-14
13 (L) 58 6.80e-14
LCAT 9 (L+M) 27 1.34e-09
9 (L) 27 1.34e-09
LDL PCSK9 31 (L+M) 245 9.19e-49
30 (L) 244 8.54e-49
ANGPTL3 33 (L+M) 363 7.98e-16
33 (L) 363 7.98e-16
APOB 85 (L+M) 237 2.94e-262
85 (L) 237 2.94e-262
GIGYF1 32 (L+M) 52 9.02e-09
32 (L) 52 9.02e-09
LDLR 32 (L+M) 98 4.06e-11
26 (L) 53 2.59e-05
Triglycerides ANGPTL3 33 (L+M) 363 2.03e-39
33 (L) 363 2.03e-39
APOB 85 (L+M) 237 3.21e-117
85 (L) 237 3.21e-117
LPL 28 (L+M) 86 4.68e-10
18 (L) 64 4.93e-09
PDE3B 44 (L+M) 224 3.63e-07
31 (L) 71 3.97e-03
APOA5 18 (L+M) 180 2.31e-36
18 (L) 180 2.31e-36
APOC3 3 (L+M) 22 1.42e-08
3 (L) 22 1.42e-08
ANGPTL4 23 (L+M) 173 1.32e-09
23 (L) 173 1.32e-09
Lipoprotein(a) LPA 83 (L+M) 307 4.30e-10
83 (L) 307 4.30e-10
Glucose GCK 20 (L+M) 56 1.91e-20
13 (L) 20 1.79e-09
GIGYF1 31 (L+M) 51 9.45e-09
31 (L) 51 9.45e-09
Igf-1 JAK2 48 (L+M) 70 1.64e-11
41 (L) 52 2.82e-11
Pulse Rate TTN 697 (L+M) 1707 8.82e-17
694 (L) 1704 6.51e-17
LVEF TTN 115 (L+M) 179 5.01e-10
115 (L) 179 5.01e-10
-2.5
-2
-1.5
-1
-0.5
0
0.5
1
1.5
2
Effect size [95% CI]

**Supplementary Figure 9. Sensitivity analysis restricting to LOFs only in the primary analysis of quantitative traits.** Data are presented as effect size (β) estimates per standard deviation with error bars representing 95% confidence intervals (CI). *P*-values, effect sizes and 95% CIs were obtained from score tests in linear mixed effects models, adjusting for sex, age, sequencing batch, associated principal components (PCs), MRI serial number (for MRI traits) and a sparse kinship matrix. *P*-values shown are two-sided and unadjusted for multiple testing. Effect estimates for analysis of LOFs were largely consistent with effect estimates from LOFs and predicted-damaging missense combined. Abbreviations: L, high-confidence loss-of-function variants only; L+M, high-confidence loss-of-function and predicted-damaging missense variants combined; CI, confidence interval; HDL, high-density lipoprotein; LDL, low-density lipoprotein; Igf-1, insulin-like growth factor-1; QTc, Bazett-corrected QT interval; LVEF, left ventricular ejection fraction; CI, confidence interval.

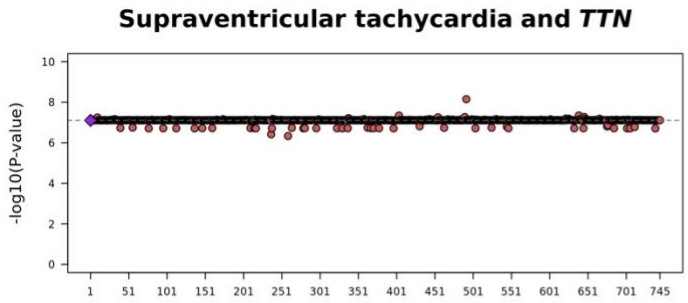
Supraventricular tachycardia and *TTN*
-log10(P-value)

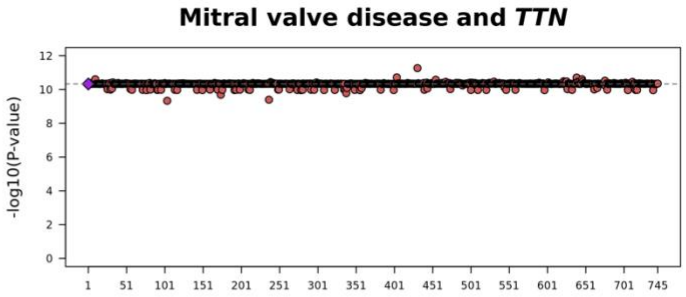
Mitral valve disease and *TTN*
-log10(P-value)

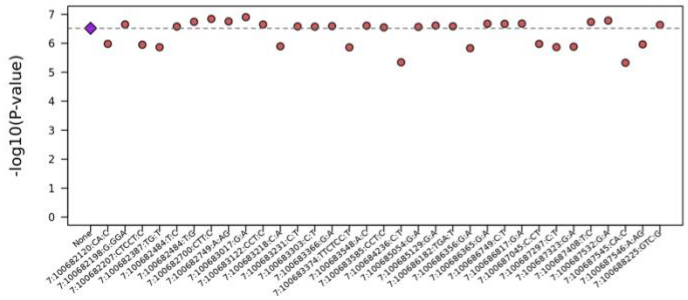
Diabetes type 2 and *GIGYF1*
-log10(P-value)

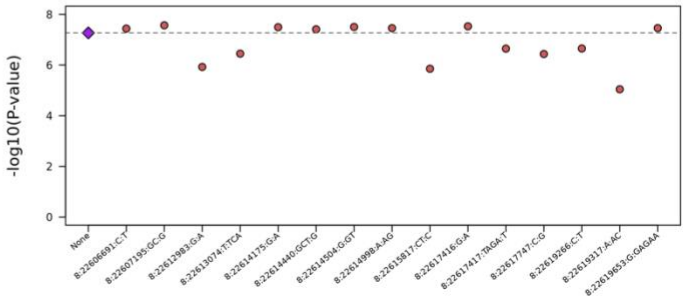
Diabetes type 2 and *CCAR2*
-log10(P-value)

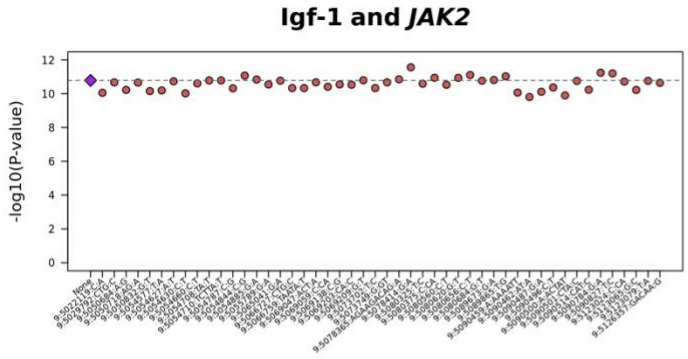
Igf-1 and *JAK2*
-log10(P-value)

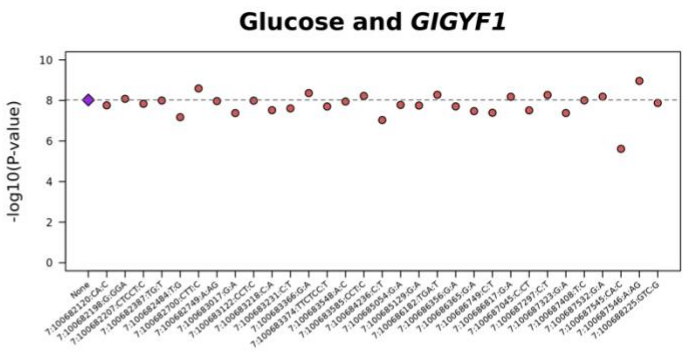
Glucose and *GIGYF1*
-log10(P-value)

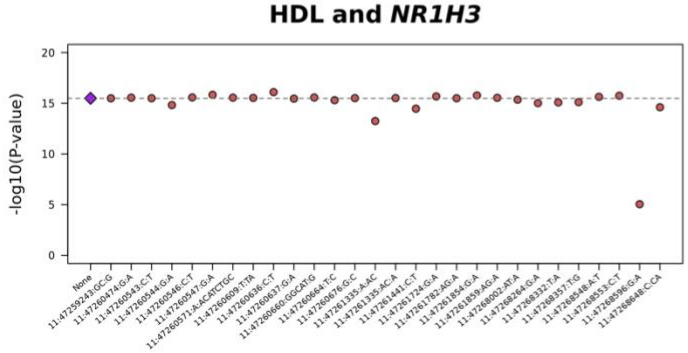
HDL and *NR1H3*
-log10(P-value)

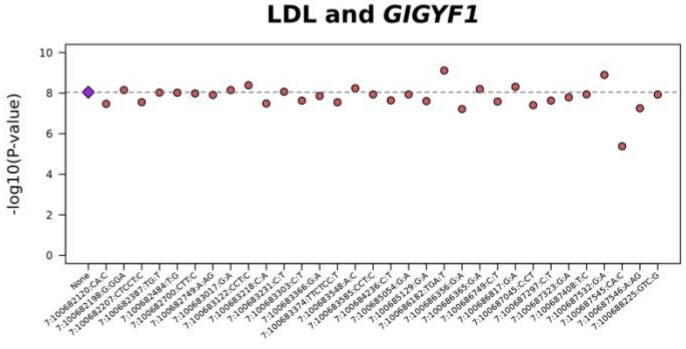
LDL and *GIGYF1*
-log10(P-value)

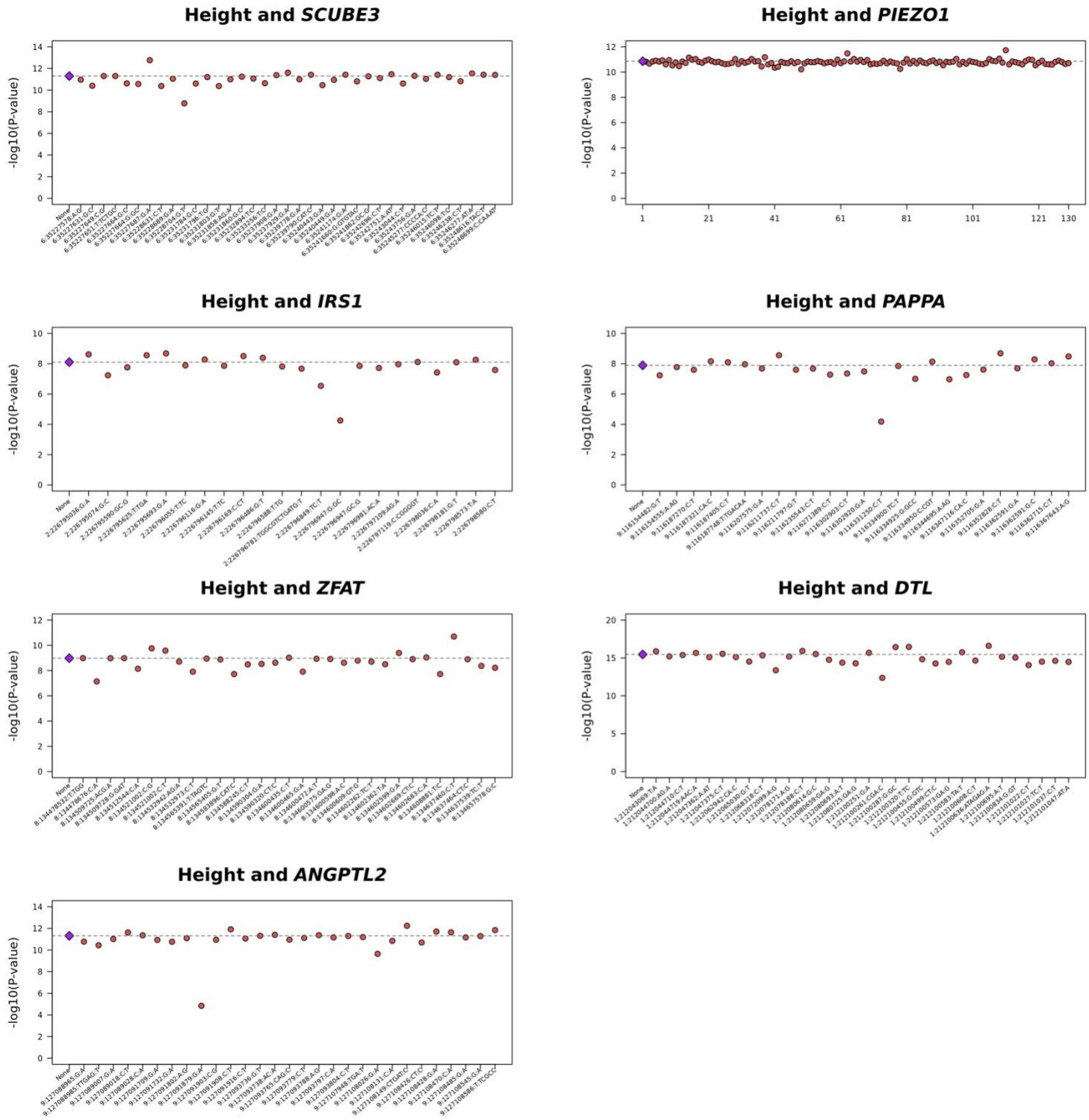


**Supplementary Figure 10. Leave-one-variant-out (LOVO) analysis for novel rare variant associations.** The x-axis represents a single variant removed from the gene-based analysis, while the y-axis shows the $-_{10}\log$ *P*-value of the association without that given variant. *P*-values were obtained from score tests in linear mixed effects models (quantitative traits) or saddle point approximation in logistic mixed effects models (binary traits), adjusting for sex, age, sequencing batch, associated principal components (PCs) and a sparse kinship matrix. *P*-values shown are two-sided and unadjusted for multiple testing. The first result (diamond) shows the original result without any variant removed. Variants are annotated with the variant name in format

chromosome:position:reference:alternative; for *TTN* variant names are not shown given the many variants in the masks. Associations are never abolished upon removing the most important variant from the mask.

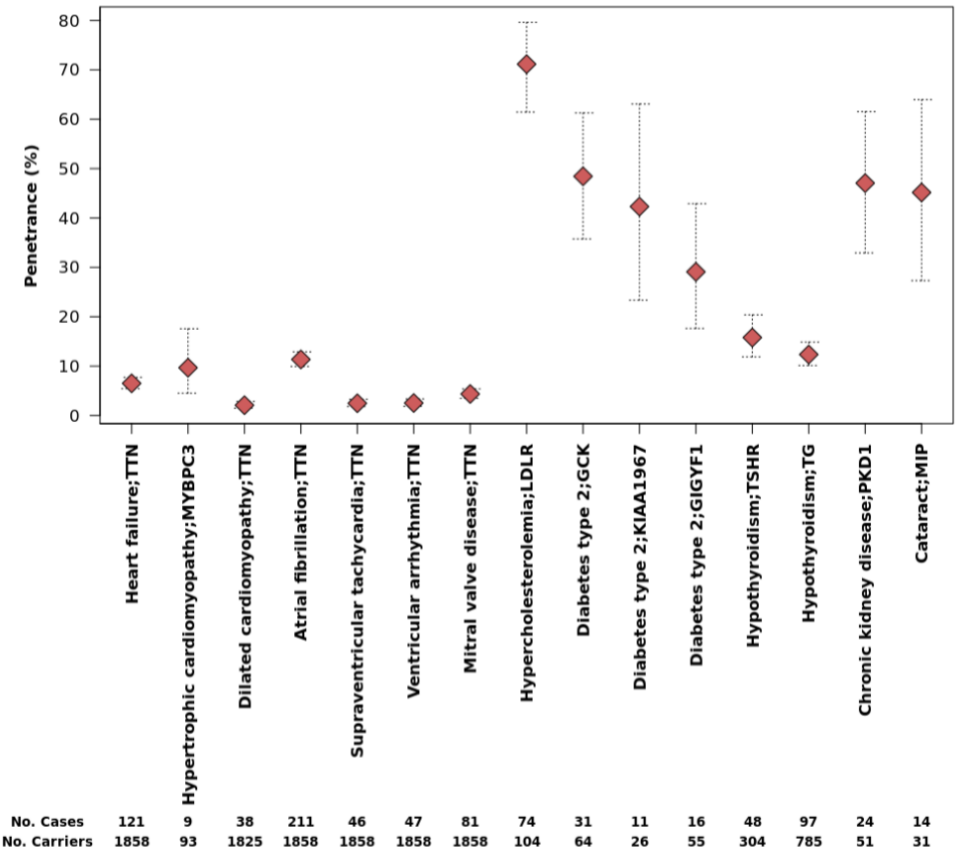


**Supplementary Figure 11. Penetrance of predicted-damaging variants in genes associated with disease in the primary analyses.** The x-axis presents gene-phenotype pairs significantly associated with increased disease risk in the primary analysis of loss-of-function and predicted-deleterious missense variants. 'Significant increased disease risk' was defined as Benjamini-Hochberg two-sided Q-value < 0.01 (computed from *P*-values from all tests in the discovery phase using saddle point approximation in logistic mixed effects models) and Odds Ratio (OR) > 1 (computed from Firth's regression models among unrelated samples). Data on the y-axis are presented as penetrance - calculated as the number of rare variant carriers who were disease cases divided by the total number of carriers times 100% - with dotted lines representing 95% exact binomial confidence intervals. Based on effect sizes, the penetrance estimates for diabetes type 2/*GCK* likely underestimate true loss-of-function, while the other associations should be comparable to loss-of-function variants estimates (**Supplementary Figure 8**).

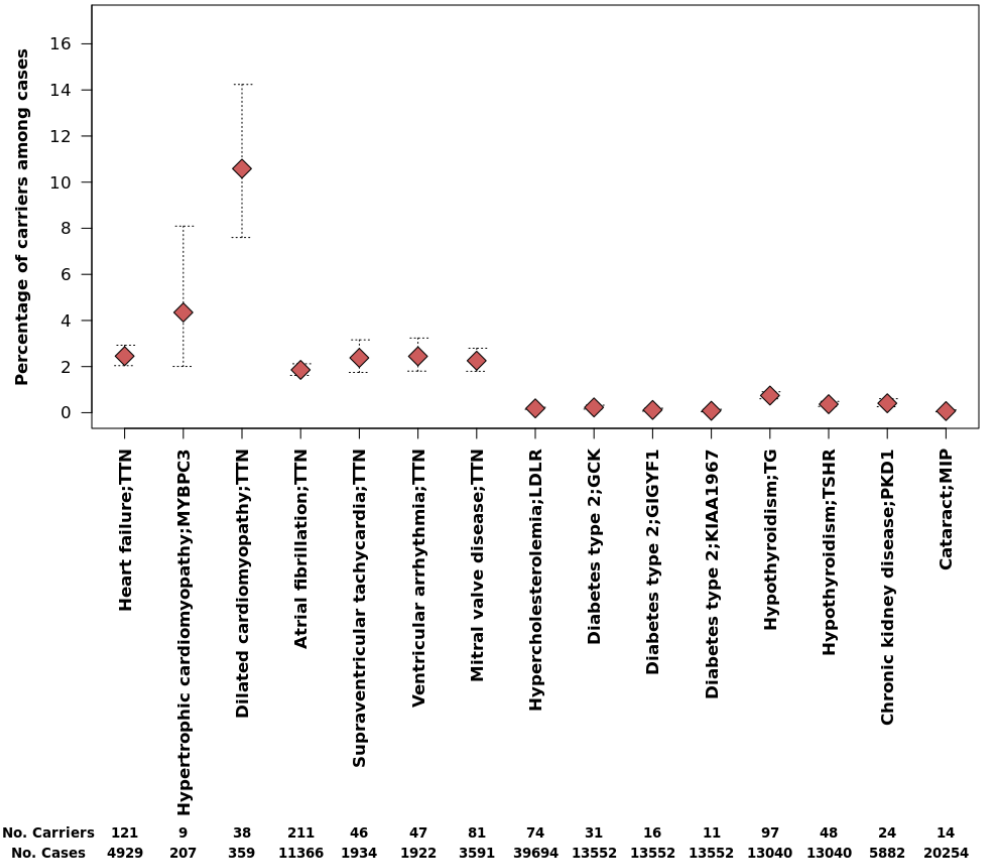


**Supplementary Figure 12. Prevalence of predicted-damaging variants in genes identified in primary analysis among relevant disease cases.** The x-axis presents gene-phenotype pairs significantly associated with increased disease risk in the primary analysis of loss-of-function and predicted-deleterious missense variants. 'Significant increased disease risk' was defined as Benjamini-Hochberg two-sided Q-value < 0.01 (computed from *P*-values from all tests in the discovery phase using saddle point approximatio in logistic mixed effects models) and Odds Ratio (OR) > 1 (computed from Firth's regression models among unrelated samples). Data on the y-axis are presented as the percentage of rare variant carriers among disease cases - calculated as the number of rare variant carriers who were disease cases divided by the total number of disease cases times 100% - with dotted lines representing 95% exact binomial confidence intervals. Among individuals with dilated cardiomyopathy, up to 12% may carry rare variants in *TTN.* In general, however, rare high-impact variants are rare among common adult-onset disease cases.

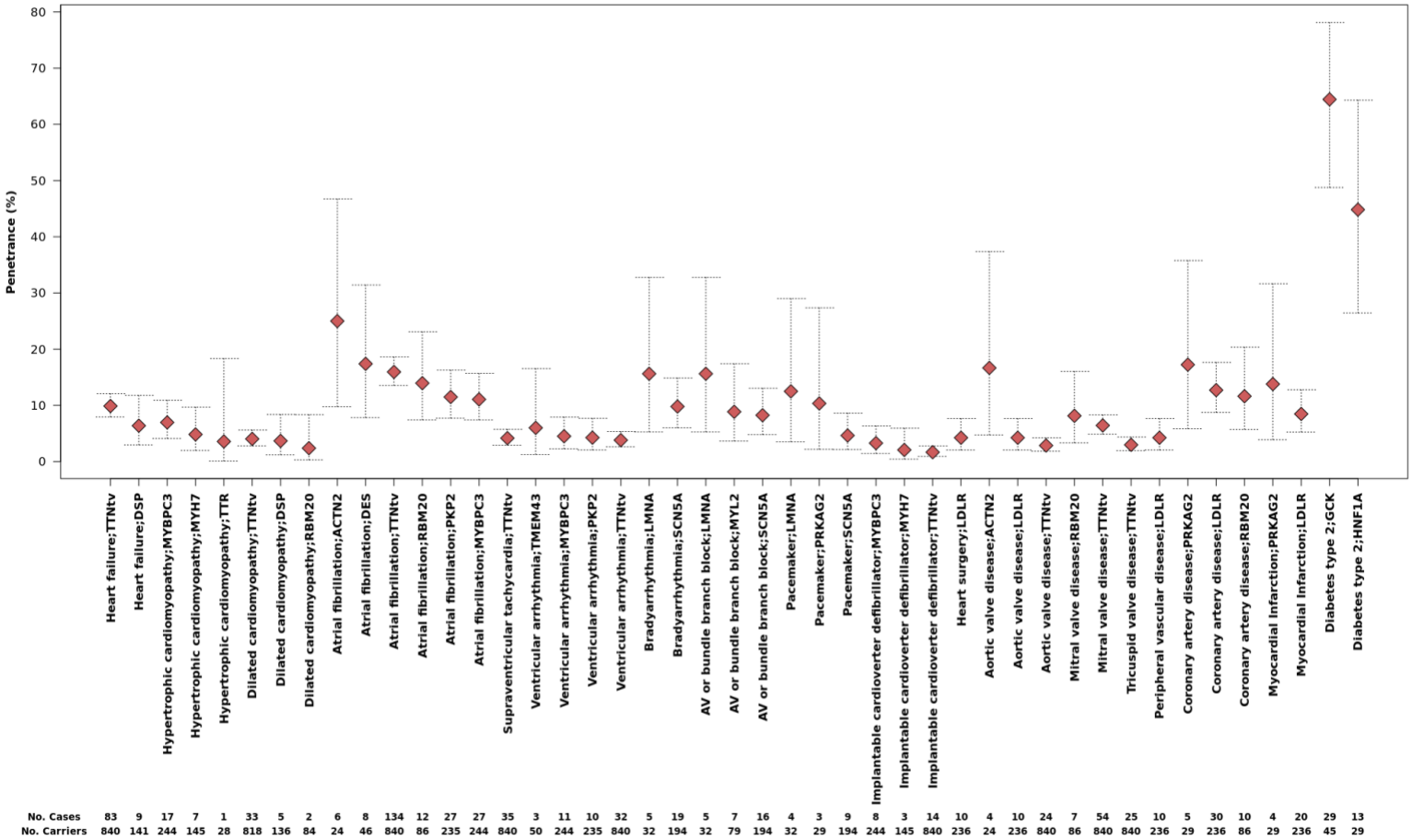


**Supplementary Figure 13. Penetrance of putatively pathogenic variants in cardiovascular disease and diabetes panel genes for relevant phenotypes.** The x-axis presents gene-phenotype pairs showing at least suggestive evidence of association with increased disease risk in the analysis of putatively pathogenic variants in cardiovascular and diabetes panel genes. 'Suggestive increased disease risk' was defined as two-sided *P*-value < 0.005 (unadjusted for multiple testing; computed using saddle point approximation in logistic mixed effects models) and Odds Ratio (OR) > 1 (computed from Firth's regression models among unrelated samples). Data on the y-axis are presented as penetrance - calculated as the number of rare variant carriers who were disease cases divided by the total number of carriers times 100% - with dotted lines representing 95% exact binomial confidence intervals.

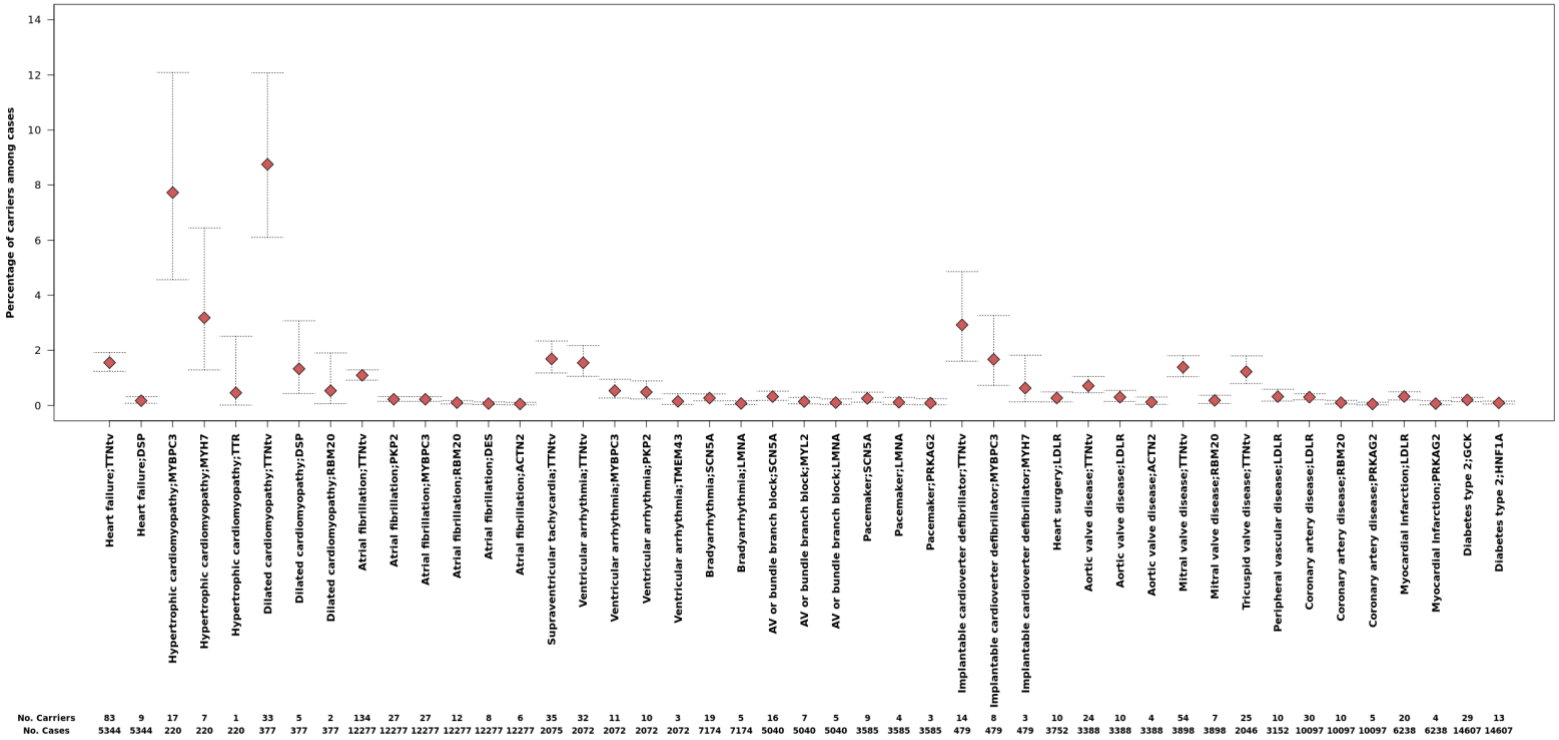


**Supplementary Figure 14. Prevalence of putatively pathogenic variants in cardiovascular disease and diabetes panel genes among disease cases.** The x-axis presents gene-phenotype pairs showing at least suggestive evidence of association in the analysis of putatively pathogenic variants in cardiovascular and diabetes panel genes. 'Suggestive increased disease risk' was defined as two-sided *P*-value < 0.005 (unadjusted for multiple testing; computed using saddle point approximation inn logistic mixed effects models) and Odds Ratio (OR) > 1 (computed from Firth's regression models among unrelated samples). Data on the y-axis are presented as the percentage of rare variant carriers among disease cases - calculated as the number of rare variant carriers who were disease cases divided by the total number of disease cases times 100% - with dotted lines representing 95% exact binomial confidence intervals.

## Supplementary References


1. Szustakowski, J.D. *et al.* Advancing Human Genetics Research and Drug Discovery through Exome Sequencing of the UK Biobank. *medRxiv* (2020).
2. Regier, A.A. *et al.* Functional equivalence of genome sequencing analysis pipelines enables harmonized variant calling across human genetics projects. *Nat Commun* **9**, 4038 (2018).
3. Yun, T. *et al.* Accurate, scalable cohort variant calls using DeepVariant and GLnexus. *Bioinformatics* **36**, 5582–5589 (2021).
4. Chang, C.C. *et al.* Second-generation PLINK: rising to the challenge of larger and richer datasets. *Gigascience* **4**, 7 (2015).
5. Bycroft, C. *et al.* The UK Biobank resource with deep phenotyping and genomic data. *Nature* **562**, 203-209 (2018).
6. Manichaikul, A. *et al.* Robust relationship inference in genome-wide association studies. *Bioinformatics* **26**, 2867-73 (2010).
7. Conomos, M.P., Miller, M.B. & Thornton, T.A. Robust inference of population structure for ancestry prediction and correction of stratification in the presence of relatedness. *Genet Epidemiol* **39**, 276-93 (2015).
8. Galinsky, K.J. *et al.* Fast Principal-Component Analysis Reveals Convergent Evolution of ADH1B in Europe and East Asia. *Am J Hum Genet* **98**, 456-472 (2016).
9. Karczewski, K.J. *et al.* The mutational constraint spectrum quantified from variation in 141,456 humans. *Nature* **581**, 434-443 (2020).
10. Type 2 Diabetes Knowledge Portal. Accessed in December 2020 and June 2021; http://www.type2diabetesgenetics.org
11. Willer, C.J., Li, Y. & Abecasis, G.R. METAL: fast and efficient meta-analysis of genomewide association scans. *Bioinformatics* **26**, 2190-1 (2010).
12. de Leeuw, C.A., Mooij, J.M., Heskes, T. & Posthuma, D. MAGMA: generalized gene-set analysis of GWAS data. *PLoS Comput Biol* **11**, e1004219 (2015).
13. Consortium, G. The GTEx Consortium atlas of genetic regulatory effects across human tissues. *Science* **369**, 1318-1330 (2020).
14. Roberts, A.M. *et al.* Integrated allelic, transcriptional, and phenomic dissection of the cardiac effects of titin truncations in health and disease. *Sci Transl Med* **7**, 270ra6 (2015).
15. Choi, S.H. *et al.* Monogenic and Polygenic Contributions to Atrial Fibrillation Risk: Results From a National Biobank. *Circ Res* **126**, 200-209 (2020).
16. Cornec-Le Gall, E. *et al.* Type of PKD1 mutation influences renal outcome in ADPKD. *J Am Soc Nephrol* **24**, 1006-13 (2013).
17. Mallawaarachchi, A.C., Furlong, T.J., Shine, J., Harris, P.C. & Cowley, M.J. Population data improves variant interpretation in autosomal dominant polycystic kidney disease. *Genet Med* **21**, 1425-1434 (2019).
18. Ali, H. *et al.* PKD1 Duplicated regions limit clinical Utility of Whole Exome Sequencing for Genetic Diagnosis of Autosomal Dominant Polycystic Kidney Disease. *Sci Rep* **9**, 4141 (2019).
19. Rossetti, S. *et al.* Identification of gene mutations in autosomal dominant polycystic kidney disease through targeted resequencing. *J Am Soc Nephrol* **23**, 915-33 (2012).
20. Trujillano, D. *et al.* Diagnosis of autosomal dominant polycystic kidney disease using efficient PKD1 and PKD2 targeted next-generation sequencing. *Mol Genet Genomic Med* **2**, 412-21 (2014).
21. Akhtar, M.M. *et al.* Clinical Phenotypes and Prognosis of Dilated Cardiomyopathy Caused by Truncating Variants in the. *Circ Heart Fail* **13**, e006832 (2020).
22. Franaszczyk, M. *et al.* Titin Truncating Variants in Dilated Cardiomyopathy - Prevalence and Genotype-Phenotype Correlations. *PLoS One* **12**, e0169007 (2017).
23. Haggerty, C.M. *et al.* Genomics-First Evaluation of Heart Disease Associated With Titin-Truncating Variants. *Circulation* **140**, 42-54 (2019).
24. Michels, M. *et al.* Disease penetrance and risk stratification for sudden cardiac death in asymptomatic hypertrophic cardiomyopathy mutation carriers. *Eur Heart J* **30**, 2593-8 (2009).
25. Viswanathan, S.K. *et al.* Hypertrophic cardiomyopathy clinical phenotype is independent of gene mutation and mutation dosage. *PLoS One* **12**, e0187948 (2017).

26. Adalsteinsdottir, B. *et al.* Hypertrophic cardiomyopathy in myosin-binding protein C (MYBPC3) Icelandic founder mutation carriers. *Open Heart* **7**, e001220 (2020).
27. Lorenzini, M. *et al.* Penetrance of Hypertrophic Cardiomyopathy in Sarcomere Protein Mutation Carriers. *J Am Coll Cardiol* **76**, 550-559 (2020).
28. Walsh, R. *et al.* Reassessment of Mendelian gene pathogenicity using 7,855 cardiomyopathy cases and 60,706 reference samples. *Genet Med* **19**, 192-203 (2017).
29. Groeneweg, J.A. *et al.* Clinical Presentation, Long-Term Follow-Up, and Outcomes of 1001 Arrhythmogenic Right Ventricular Dysplasia/Cardiomyopathy Patients and Family Members. *Circ Cardiovasc Genet* **8**, 437-46 (2015).
30. Patel, K.A. *et al.* Heterozygous RFX6 protein truncating variants are associated with MODY with reduced penetrance. *Nat Commun* **8**, 888 (2017).
31. Chakera, A.J. *et al.* Recognition and Management of Individuals With Hyperglycemia Because of a Heterozygous Glucokinase Mutation. *Diabetes Care* **38**, 1383-92 (2015).
32. Wang, Z. *et al.* Identification and functional analysis of GCK gene mutations in 12 Chinese families with hyperglycemia. *J Diabetes Investig* **10**, 963-971 (2019).
33. Bansal, V. *et al.* Spectrum of mutations in monogenic diabetes genes identified from high-throughput DNA sequencing of 6888 individuals. *BMC Med* **15**, 213 (2017).
34. Wright, C.F. *et al.* Assessing the Pathogenicity, Penetrance, and Expressivity of Putative Disease-Causing Variants in a Population Setting. *Am J Hum Genet* **104**, 275-286 (2019).